Journal of Hydrology 667 (2026) 134879

Contents lists available at ScienceDirect

Journal of Hydrology

journal homepage: www.elsevier.com/locate/jhydrol

Research papers

The trend and interannual variability in the global terrestrial evapotranspiration are respectively dominated by humid regions and drylands

Huiling Chen [a,b], Kun Zhang [c,*], Gaofeng Zhu [b,*], Lei Fan [d], Xin Li [e], Yunquan Wang [f], Xufeng Wang [g], Shasha Shang [h], Jia Jia [a], Yongtai Zhu [b], Jingfeng Xiao [i]

[a] College of Geography and Environmental Sciences, Zhejiang Normal University, Jinhua, China
[b] College of Earth and Environmental Sciences, Lanzhou University, Lanzhou, China
[c] School of Geospatial Engineering and Science, Sun Yat-sen University, Zhuhai, China
[d] Chongqing Jinfo Mountain Karst Ecosystem National Observation and Research Station, School of Geographical Sciences, Southwest University, Chongqing, China
[e] National Tibetan Plateau Data Center (TPDC), State Key Laboratory of Tibetan Plateau Earth System, Environment and Resources (TPESER), Institute of Tibetan Plateau Research, Chinese Academy of Sciences, Beijing, China
[f] Hubei Key Laboratory of Yangtze River Basin Environmental Aquatic Science, School of Environmental Studies, China University of Geosciences at Wuhan, Wuhan, China
[g] Key Laboratory of Remote Sensing of Gansu Province, Heihe Remote Sensing Experimental Research Station, Northwest Institute of Eco-Environment and Resources, Chinese Academy of Sciences, Lanzhou, China
[h] Tianjin Key Laboratory of Water Resources and Environment, Tianjin Normal University, Tianjin, China
[i] Earth Systems Research Center, Institute for the Study of Earth, Oceans, and Space, University of New Hampshire, Durham, NH 03824, USA

ARTICLE INFO

This manuscript was handled by Amilcare Porporato, Editor-in-Chief

Keywords:
Land evapotranspiration dynamics
Long-term trend
Short-term interannual variability
ENSO
Climate warming
Vegetation greening

ABSTRACT

Despite characterized by large interannual variability (IAV), global terrestrial evapotranspiration (ET) has existed a consistent increasing trend since the 1980s. However, the regions and processes governing the present ET trend and IAV still remain unclear. Using an ensemble of process-based hydrological models, remote sensing-based, machine learning, and land surface products, we find that the increasing trend and substantial IAV in global land ET are driven by divergent regions. Result from models ensemble shows that the humid regions, especially in the Northern Hemisphere, contribute the 72.47 ± 5.77 % of the increase in global land ET over 1982–2020. In this domain, climate warming and vegetation greening (increased leaf area index (LAI)) have caused the increase in ET of 0.43 ± 0.22 and 0.30 ± 0.13 mm yr^{-2}, respectively, although the increased LAI is the largest contributions (63.69 ± 25.13 %) to the global ET increases. Especially, climate warming in the humid regions at the high latitudes has prolonged the growing season, and provided sufficient water through freeze–thaw process for the enhanced plants photosynthesis in spring and even summer. The IAV of the global land ET, however, is dominated by drylands (with contribution fractions being 59.66 ± 16.89 %), and dominant role in this region is mainly due to the fact that the precipitation, which serves as a primary source of moisture supply, has the large interannual oscillation with the El Niño/Southern Oscillation (ENSO) events and is largely allocated to evaporation. With future anthropogenic warming, global land ET is expected to continue rising with the trait of a significant interannual variations, and the dominant roles of humid regions and drylands still remains and are stronger than that in present. This study will merit more attention about regional roles for understanding and projecting dynamics of the global water cycle.

1. Introduction

Land evapotranspiration (ET) plays a critical role in linking the water, energy and carbon cycles (Oki and Kanae, 2006; Fisher et al., 2017; Allan et al., 2020). Its changes can strongly alter the global patterns of precipitation (Mondal et al., 2024; Hofmann et al., 2023; Gao et al., 2025) and temperature (Teuling, et al., 2013; Leggett and Ball, 2019), influence the occurrence of extreme events, such as droughts,

* Corresponding authors.
E-mail addresses: zhangkun3@mail.sysu.edu.cn (K. Zhang), zhugf@lzu.edu.cn (G. Zhu).

https://doi.org/10.1016/j.jhydrol.2025.134879
Received 14 October 2025; Received in revised form 23 December 2025; Accepted 26 December 2025
Available online 27 December 2025

floods and heatwaves (Zhao et al., 2022; Vicente-Serrano et al., 2025; He et al., 2025), and at the regional scale, affect terrestrial ecosystems, watershed hydrological cycles, agricultural irrigation, and the allocation of watershed water resources (Padrón et al., 2020; Zhang et al., 2023; Volk et al., 2024). Furthermore, the ET changes are fundamentally driven by variations in atmospheric moisture demand (i.e., temperature, radiation and vapor pressure deficit), water supply (i.e., precipitation and soil moisture), and vegetation dynamics (Jung et al., 2011; Miralles et al., 2014; Zeng et al., 2018; Yang et al., 2023; Liu et al., 2025; Zhu et al., 2025). These climatic and ecological factors vary over space and time, and can lead to substantial differences in regional ET and consequently affect global terrestrial ET. Therefore, synthetically understanding the changes in regional and global land ET and its causes is essential for understanding the exchanges of energy, water and carbon between the earth surface and atmosphere, as well as the responses to human activities, climate changes, and extreme weather events (Condon et al., 2020; Scanlon et al., 2023; Zhang et al., 2023; Graveline et al., 2024; Camps-Valls et al., 2025).

Considerable attention has been paid to explore the land ET changes through remote sensing retrieval, model simulation, and machine learning (Jung et al., 2011; Fisher et al., 2017; Zhang et al., 2024; Wang et al., 2022; Tang et al., 2024; Xue et al., 2025; Miralles et al., 2025). Most of the above studies agreed on an overall increase in land ET from 1982 to the early 2010 s, but with the substantial interannual variability (IAV). However, the trend and IAV components of the land ET series were lumped together in most previous studies, failing to elucidate the impacts of their interactions on the short-term fluctuations of land ET (Egli et al., 2024). Thus, some conflicting conclusions about long-term trend and responses to short-term variability have arisen based on data spanning different periods. For instance, some studies posited a cessation of increasing land ET from 1998 to 2008 (Jung et al., 2011; Douville et al., 2013), while other studies with extended records indicate this phenomenon to be episodic, with a subsequent recovery of land ET after 2008 (Zhang et al., 2016; Pan et al., 2020; Yang et al., 2023; Xue et al., 2025). Meanwhile, there are large uncertainties in the magnitude and spatio-temporal patterns of ET estimates, linked to the inability to observe ET directly from satellite sensors, limited coverage by in situ ET observations and difficulty in parameterizing the complex and intertwined physical and biological processes governing ET at different scales (Miralles et al., 2025). Therefore, reducing the uncertainty of the changes of global land ET requires better knowledge of regions and process driving the present ET trend and interannual variations.

Moreover, previous studies attributed the increasing trend in global land ET to the temperature warming (Wang et al., 2022; Pan et al., 2015; Miralles et al., 2014), moisture supply (Jung et al., 2011; Yan et al., 2013), vegetation greening (Zhang et al., 2015; Zeng et al., 2018; Piao et al., 2019; Yang et al., 2023; Aguilos et al., 2024; Liu et al., 2025), etc., indicating that the mechanism governing the trend of land ET is not yet fully characterized. For the interannual variability, studies have shown that the ET IAV are largely related to climate events, such as the El Niño/Southern Oscillation (ENSO), which alters the global patterns of temperature and precipitation, and even vegetation dynamics (Yan et al., 2013; Miralles et al., 2014; Tito et al., 2020; Zhang et al., 2020; Palácios et al., 2024). Some studies reported that negative ET anomalies occur during El Niño due to the moisture supply limitations and vegetation water stress, and the opposite situation occurs during La Niña (Yan et al., 2013; Miralles et al., 2014; Yang et al., 2023). However, other studies found that the positive ET anomalies occurred during the El Niño events (Purdy et al., 2018; Zhang et al., 2020), duo to the increased atmosphere moisture evaporation. Short-term climate anomalies can affect the regional ET variations, and also produce the influence on the long-term trend of ET, resulting in high uncertainty in the changes of ET at the regional and global levels (Vicente-Serrano et al., 2022; Dorigo et al., 2021; Zhao et al., 2022). Therefore, attributing the regions governing the present land ET trend and IAV can better project future water cycle.

Here we examine the dominant regions driving both the long-term trends and IAV of global land ET from the early 1980 s to 2020, along with their underlying mechanisms. We use an ensemble of process-based hydrological model (Simple Terrestrial Hydrosphere model version 2, SiTHv2) (Zhu et al., 2019; Zhang et al., 2024), and other remote sensing-based, machine learning, and land surface products of global land ET, to identify the regions driving the overall land ET trend. These independent ET products include the five independent modelling products and simulations from 20 Earth System Models (ESMs) that participated in the Coupled Model Inter-comparison Project Phase 6 (CMIP6) (Eyring et al., 2016). Our scientific objectives were: 1) to identify the regions that control the global land ET trend and IAV; 2) to explore the mechanisms that influence the dynamic changes (trend and IAV) of global ET; and 3) to predict whether the dominant regions for the dynamic changes of global terrestrial ET will change in the future.

2. Materials and methods

2.1. Model forcing data

Here we use the SiTHv2 model as the core methodology for our analysis of ET for 1980–2020, with derived global trends and IAVs contrasted against ET estimates from a range of different models. For the SiTHv2 model, the main input variables include the meteorological variables of air temperature (T_a), net radiation (R_n), and precipitation (P), vegetation dynamics (leaf area index (LAI) and land cover), and soil texture data. In this study, one set of long-term continuous input datasets, as a reference ET data, is applied to drive the SiTHv2 model. We employed daily air temperature and air pressure data from the Multi-Source Weather (MSWX) product (Beck et al., 2022), a bias-corrected meteorological dataset with a spatial resolution of 0.1° since 1979. The Multi-source Weighted Ensemble Precipitation (MSWEP; Beck et al., 2019) generated precipitation datasets with a temporal resolution of 3 h and a spatial resolution of 0.1°, which were estimated by comprehensive diurnal scale observations and satellite reanalysis. The net radiation dataset stem from the latest ERA5-land products (Muñoz-Sabater et al., 2021). This dataset is produced by the European Centre for Medium-Range Weather Forecasts (ECMWF), with an 0.1° spatial resolution and an hourly temporal resolution since 1979. We utilized the LAI datasets from a new version of the half-month 1/12° Global Inventory Modeling and Mapping Studies (GIMMS) LAI product (GIMMS LAI4g) (Cao et al., 2023), which stems from the GIMMS NDVI product, Landsat LAI samples and the reprocessed MODIS LAI product using machine learning models and a data consolidation method. We acquired long-term land cover dynamics at an annual scale from the Historic Land Dynamics Assessment+ (HILDA+) product (Winkler et al., 2021), a compressive land cover/use product that integrates multiple open data sources, encompassing remote sensing, reconstructions, and statistics. Finally, the required static soil texture dataset was derived from the FAO Harmonized World Soil Database (HWSD) at 0.1° spatial resolution.

Additionally, to increase the confidence in our findings and quantify the level of uncertainty, we performed the another four set of forcing datasets to obtain ET estimations for SiTHv2 model. The four experiments respectively use alternative data set of LAI (e1), air temperature (e2), precipitation (e3), and net radiation (e4)—see Table S1 for a detailed description of these experiments.

2.2. The ET data employed for the comparison

2.2.1. Flux towers ET data

We evaluated the accuracy of SiTHv2 estimates from multiple scales, i.e. in-situ observations, water-balanced ET at basins, and global grid-based ET. Specifically, we validated the total ET estimates of SiTHv2 using latent heat flux measurements from 137 global eddy covariance (EC) stations with a daily interval. These EC stations encompass nine major plant functional types under various climate conditions (Fig. S1). The quality flags of the latent heat flux (LE_F_MDS_QC) must be higher

than 0.75. Moreover, the surface energy closures at least are above 70 % (Fig. S2).

2.2.2. Water-balanced ET products at river basin

We utilized water-balance-based ET estimation (ETwb) product produced by Ma et al. (2024) to validate SiTHv2-based ET estimates at a basin scale. Using remote sensing and ground-based observational data, this ETwb dataset derived from the residual of the basin water balance equation (precipitation minus runoff and changes in total water storage from GRACE data), provides ET estimations for a total of 56 large ($>10^5$ km^2) river basins over the 1983–2016 period that covering a broad range of climate zones globally.

2.2.3. Other ET products

For an inter-comparison of the SiTHv2 ET at global scale, five mainstream ET products (Table 1) are selected among the following five categories. One widely used process-based datasets is selected: the Global Land Evaporation Amsterdam Model (GLEAM; Miralles et al., 2025). The calibration-free complementary relationship (CR) model (Ma et al., 2021) is acquired, which is only driven by routine meteorological forcing for large-scale ET simulations. The model tree ensembles (MTE) product (Jung et al., 2011) is estimated from upscaling global flux observations to global ET through machine learning method. One reanalysis ET product, ERA5-Land (Muñoz-Sabater et al., 2021) generated the high spatial (0.1°) and temporal resolution (half-hourly) of global land ET. One land surface model from GLDAS employed is the Noah Land Surface Model (Noah_GL; Beaudoing et al., 2019), which assimilates multi-source observations and simulations of land surface models to generate credible surface states and fluxes.

Additionally, we further employed 20 CMIP6 (Eyring et al., 2016) models for auxiliary comparison, which overlaps the spanning time at 1982–2014. For each model, the ensemble member "r1i1p1" was used. Further information about the selected CMIP6 models can be found in Table S2.

2.3. SiTHv2 model description

Based on the framework of the groundwater-soil–plant-atmosphere continuum (GSPAC), the SiTHv2 model integrates well-established hydrological processes to estimate critical hydrological variables (i.e., ET, groundwater, soil moisture, and runoff) (Zhu et al., 2019; Zhang et al., 2024). In the SiTHv2 model, the total ET is partitioned between the canopy interception (E_i), soil evaporation (E_s), and plant transpiration (T_r). The soil evaporation takes place in the first soil layer, while the plant transpiration can utilize the water from the two soil layers and even groundwater. The ET components are calculated as:

$$E_i = f_{wet} \times \alpha \frac{\Delta}{\Delta+\gamma} \frac{R_{nc}}{\lambda} \tag{1}$$

$$E_s = f_{sm} \times \alpha \frac{\Delta}{\Delta+\gamma} \frac{(R_{ns}-G)}{\lambda} \tag{2}$$

$$T_r = f_v \cdot f_t \cdot \left[\sum_{i=1}^{n} \left(f_{smv,i} \cdot T_{ps,i} \right) + \sum_{i=1}^{n} T_{pg,i} \right] \tag{3}$$

where i is the soil layer (i = 1, 2); α is the Priestley-Taylor coefficient (1.26); Δ is the slope of the saturated vapor pressure curve (kPa ℃$^{-1}$); γ is the psychrometric constant, which is set to 0.066 (kPa ℃$^{-1}$); λ is the latent heat of evaporation (MJ kg^{-1}); R_{nc} and R_{ns} are the net radiation for the canopy and surface soil (W m^{-2}), respectively; G is the soil heat flux (W m^{-2}); $T_{ps,i}$ and $T_{pg,i}$ are, respectively, the potential transpiration from soil water and groundwater in the ith layer, which are calculated using the Priestley-Taylor potential ET by taking the vertical distribution of the plant roots and the position of the groundwater table into account; f_{wet} is the relative surface wetness (unitless); the f_v and f_t are the vegetation water content and temperature constraint on plant growth, respectively; f_{sm} is the soil moisture constraint (unitless); the $f_{smv,\,i}$ is the soil moisture constraint of plant transpiration at ith soil layer; More further details can be seen from Zhang et al. (2024).

Previous studies have proved that the SiTHv2 model has relatively good performances in simulating total ET and its components across different ecosystem types and climate environments (Chen et al., 2020, 2022; Zou et al., 2023; Zhang et al., 2024; Shang et al., 2024). In this study, we still evaluated the performance of ET estimations at multiple scales for SiTHv2 model. The validity of our data-driven ET product from SiTHv2 model is supported by internal cross-validation at FLUXNET sites (Fig. 1a), corroboration against independent ET estimates from catchment water balances (Fig. 1b), and spatial and latitudinal patterns of simulations of independent ET models and ensemble of 20 CMIP6 models (Fig. 1c). Based on multi-scale (sites, catchments, and global) verification (Fig. 1 and Supplementary Figs. S1-S2), the SiTHv2 model has excellent simulation performance compared to the current mainstream ET products.

2.4. Multiple linear regression method

To quantify the contribution of environmental factors to terrestrial ET, we use the historical data (1982–2020) to construct the multiple linear regression method of the interannual differences in ET against the interannual differences in the growing-season-averaged LAI (ΔLAI), annual average air temperature (ΔT_a), and annual precipitation (ΔP). The climate data and LAI data used in the multiple linear regression equation are the same as data forcing the SiTHv2 model.

$$\Delta ET = \beta 0 + \frac{\partial ET}{\partial T_a}\Delta T_a + \frac{\partial ET}{\partial P}\Delta P + \frac{\partial ET}{\partial LAI}\Delta LAI \tag{4}$$

where $\partial ET/\partial LAI$, $\partial ET/\partial P$, $\partial ET/\partial T_a$ are sensitivities of ET to changes in LAI, P and T_a, respectively. ε is the residual, representing the impacts of other factors.

Then, the effects of trend in ET induced by the changes in LAI (δET^{LAI}), P(δET^{P}), and T_a (δET^{T}_a) are quantified by multiplying the three sensitivities with trends in LAI, P and T_a, respectively. Using the following equation:

$$\delta ET^{X} = \frac{\partial ET}{\partial X} Trend_X \tag{5}$$

2.5. Statistical analysis

The contribution of the different regions to the global ET trends

Table 1
Descriptions of the ET products for comparison in this study.

ET product	Category	Temporal resolution	Spatial resolution	Temporal coverage	Reference
GLEAM	Remote sensing model	Daily	0.25°	1982–2020	Miralles et al. (2025)
CR	Complementary relationship model	Monthly	0.25°	1982–2016	Ma et al. (2021)
MTE	Machine learning model	Monthly	0.50°	1982–2011	Jung et al. (2010)
ERA5-Land	Reanalysis	Monthly	0.1°	1982–2020	Muñoz-Sabater et al. (2021)
Noah_GL	Land surface model	Monthly	0.25°	1982–2014	Beaudoing and Rodell (2019)
CMIP6	Earth System models	Monthly	0.5°	1982–2014	Eyring et al. (2016)

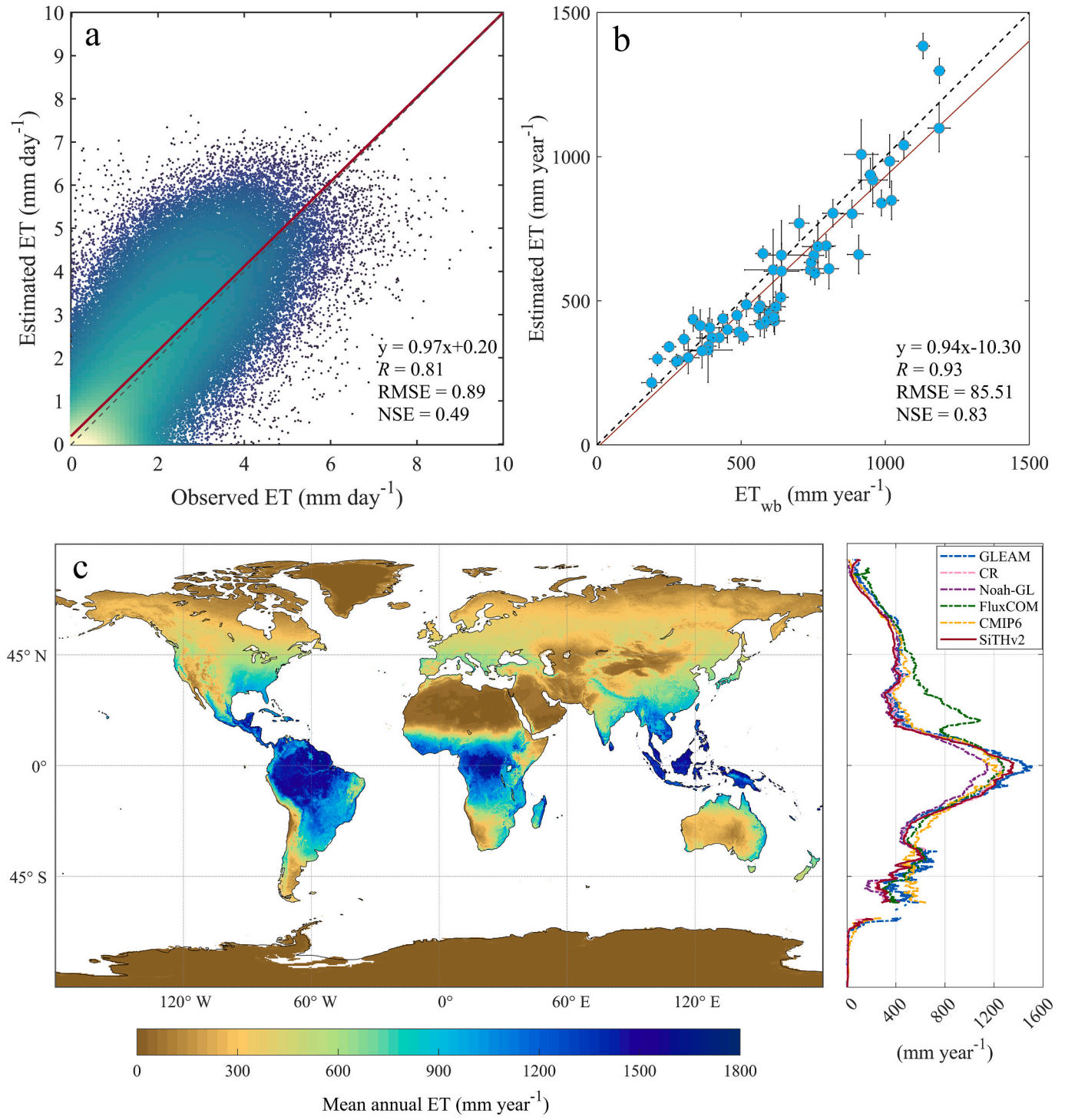

Fig. 1. Validation of global land ET product from SiTHv2. (a) Performance of SiTHv2 in daily ET estimations compared with site observations (137 flux sites). (b) Comparison of mean annual SiTHv2 ET against mean annual ET from 56 river basins based on water-balanced equation (ETwb). (c) Map of mean annual ET from SiTHv2, and zonally mean profile of annual ET from SiTHv2 and other ET products. The *R* is the Pearson's correlation coefficient, RMSE is root mean square error, and NSE is dimensionless Nash-Sutcliffe Efficiency.

(CR_{trend}) is calculated as follows:

$$CR_{trend}(j) = \frac{\sum_{i=1}^{n} Trend_{ji} \times A_{ji}}{\sum_{g=1}^{Ng} Trend_g \times A_g} \quad (6)$$

where i represents a pixel with a significant trend in region j; n is the total number of pixels in region j; $Trend_{ji}$ is the ET trend of pixel i in region j; A_{ji} is the area of a pixel i in region j, which varies with latitudes; N_g is the total number of grid cells over the global land; $Trend_g$ is the ET trend of pixel g in global; A_g is the area of a pixel g in global land.

In addition, we further explored the contribution of individual regions to the IAV in global land ET (CR_{IAV}) (Ahlström et al., 2015):

$$CR_{IAV}(j) = \frac{\sum_t \frac{ET_{jt}|ET_t|}{ET_t}}{\sum_t |ET_t|} \quad (7)$$

where ET_{jt} is the flux anomaly (departure from a long-term trend) for region j at time t (in years), and ET_t is the global flux anomaly.

3. Results and discussion

3.1. Spatial-temporal patterns of ET changes

3.1.1. Global land ET changes

Spatially, about two-third of the global land surface shows a positive ET trend (Miralles et al., 2014; Zhang et al., 2016; Yang et al., 2023; Tang et al., 2024; Xue et al., 2025), with half of these regions exhibiting significant growth (Fig. 2a). Notably, 62.4 % of areas with positive trend are distributed in the humid regions (the regions with the aridity index (AI), the ratio of annual precipitation to potential evapotranspiration, are greater than 0.65; Fig. S5), such as east America, west Europe, north Asia, southeast China, and north of South America (Fig. 2a). Zonally, the positive ET trend mainly appears in the northern latitudes, consistent with previous studies (Miralles et al., 2014; Yang et al., 2023; Tang et al., 2024). On the other hand, about one-third of the global land surface shows a negative ET trend (with significant level at 10 % areas), and the majority of these regions (~90 %) occur in the drylands (the regions with the AI < 0.65), such as west America, Arabian Peninsula, southern south America, southern eastern Africa, and south Australia (Fig. 2a). The spatial and latitudinal patterns of global ET trend from SiTHv2 sets are broadly consistent with that from the other ET products and the CMIP6 models (Fig. S6).

The spatial patterns of the global land ET IAV are displayed in Fig. 2b. The high values of IAV mainly occur in drylands, such as Southwest United States, South Africa, Sahel, Patagonia, Southern Africa, and Australia (Pan et al., 2020). Due to moisture limitation and extremely scarce precipitation (Jung et al., 2011), the hyper-arid regions, such as the Sahara and Arabian Peninsula, show the minimum ET IAV. In addition, the low ET IAV mainly occurs in humid regions, such as northern mid-high latitudes and tropical rainforest. Zonally, the value of ET IAV in south of 30°N is obviously higher than that in the north of 30°N. The spatial pattern of the IAV in ET from SiTHv2 model is broadly consistent with that from selected ET products (Fig. S7), but generally of higher magnitude than machine learning and CMIP6 ESMs (Yang et al., 2023; Tang et al., 2024).

To increase the confidence in our findings, the water-balance-derived observed ET data, that is the precipitation minus runoff and the change in terrestrial water storage within the basin (Ma et al., 2024), is selected to validate our results. For the spatial patterns of ET trend, it observed that ET exhibits an increasing trend in the majority of basins situated within humid regions, whereas a decreasing trend in drylands (Fig. 2c). Meanwhile, the spatial patterns of global land ET IAV derived from the water-balance-derived ET are consistent with that from SiTHv2 model (Fig. 2d), showing that ET IAV is high in drylands and low in humid regions of the Northern Hemisphere.

3.1.2. Humid regions dominate the trend in global land ET

The global terrestrial ET based on the SiTHv2 model increases significantly during 1982–2020, with a linear trend of 0.51 mm yr^{-2} ($p < 0.05$). The positive trend is almost identical with the ensemble mean (0.45 ± 0.13 mm yr^{-2}, $p < 0.05$) of the selected ET products (Fig. 3a). Also, the majority of the CMIP6 models exhibit an increasing trend in the global terrestrial ET, with an ensemble mean of 0.39 ± 0.18 mm yr^{-2} (Table S3). The annual mean ET in humid regions accounts for the 72.47 ± 5.77 % of that in global land (Fig. 3b). Meanwhile, the ET in humid

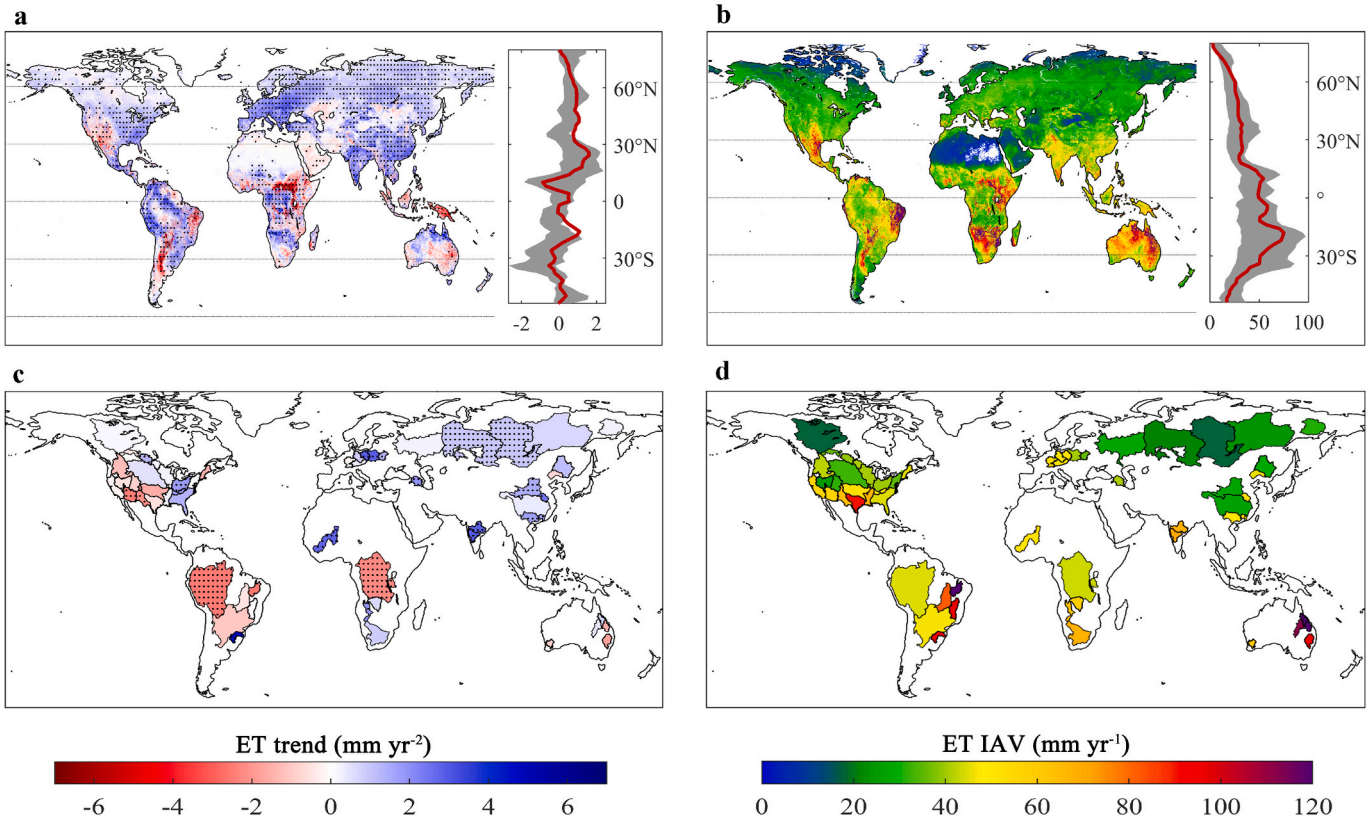

Fig. 2. Trends and IAV in global land evapotranspiration. (a-b) Spatial and latitudinal patterns of ET trends and multi-year mean ET IAV for 1982–2020 period, respectively. The red line in plot (a) represents median values of ET trend over a 2° latitudinal band. The gray shaded band in plots a and (b) show the range of ET trends and IAV from 20 CMIP6 models and other ET date sets, respectively. (c-d) The spatial patterns of ET trends and IAV from observed water-balance ET data set for 1983–2016 period. The black dots in plots ((a) and (c)) indicate where the trend is statistically significant (Mann-Kendall test, p-value < 0.05). (For interpretation of the references to colour in this figure legend, the reader is referred to the web version of this article.)

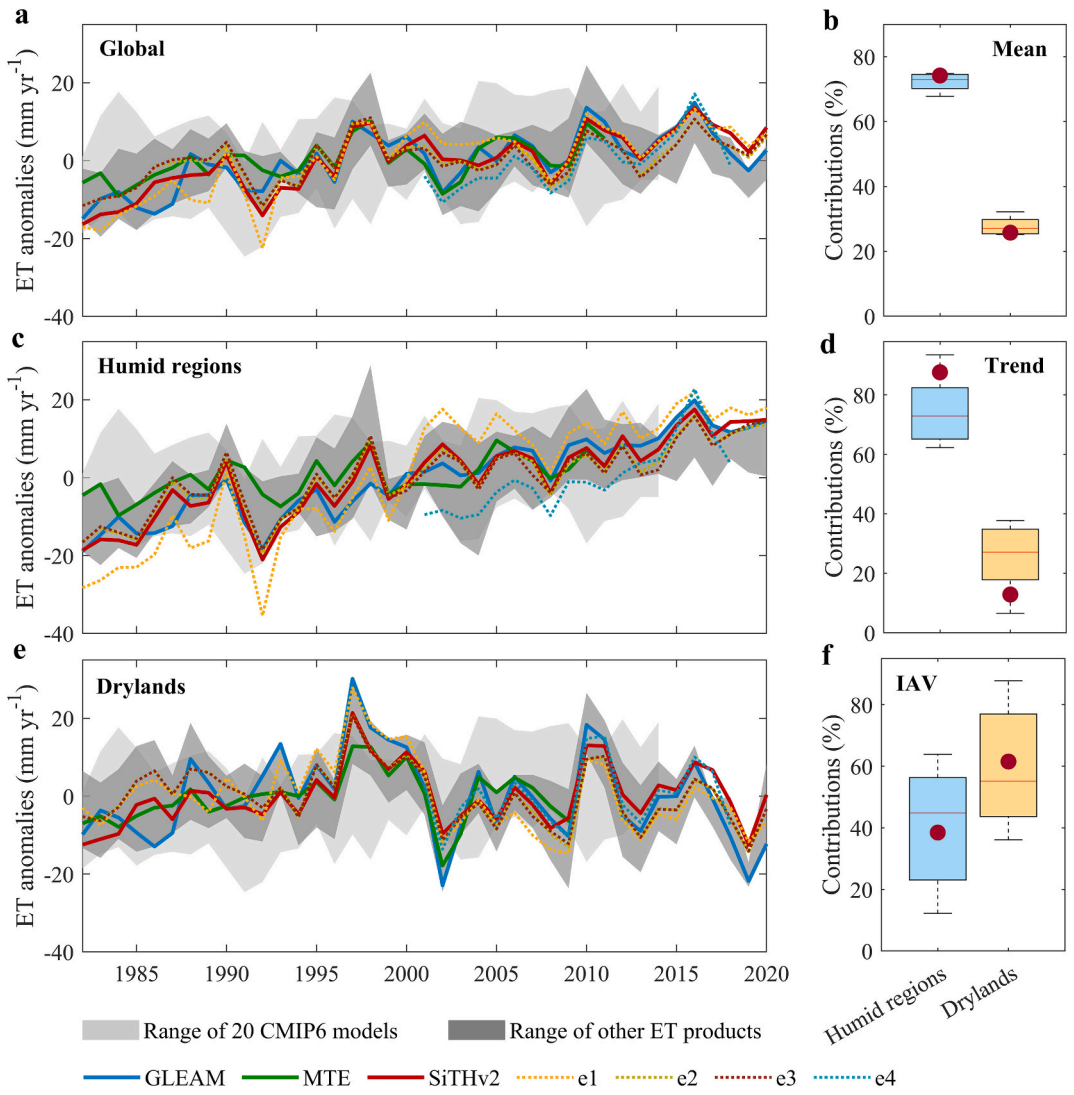

Fig. 3. Anomalies in global and regional evapotranspiration. (a), (c) and (e) Time series of annual ET in global, humid regions and drylands, respectively. The gray and dark gray shaded band in plots shows the range of ET trends from 20 CMIP6 models and other ET date sets in Table S1. The experiments e1–e4 correspond to different sets of inputs in SiTHv2 model. (b), (d), and (f) Contribution of land cover classes to global mean ET, trend ET, and IAV ET in humid and drylands, respectively. Horizontal lines inbox plots show, from top to bottom, 95th, 75th, 50th, 25th, and 5th percentiles. The red dots represent the contributions from SiTHv2 model. (For interpretation of the references to colour in this figure legend, the reader is referred to the web version of this article.)

regions estimated from SiTHv2 and other independent models also exhibit significant increasing ET trend, and the rate are higher than that in global land, with the positive trend being 0.79 mm yr^{-2} for SiTHv2 model, 0.70 ± 0.28 mm yr^{-2} for independent models, and 0.42 ± 0.23 mm yr^{-2} ($p < 0.05$) for CMIP6 models (Fig. 3c). By contrast, the ET in drylands shows no clear ET trend with strong interannual variations (Fig. 3e).

Totally, the humid regions contribute the largest fraction (75.35 ± 18.46 %) of the increase in global land ET (Fig. 3d). The drylands only make minor contributions (25.50 ± 11.22 %) to the trend. Similarly, the results from the CMIP6 models also indicate that the humid regions drive the global ET trend (56.40 ± 25.35 %), and the drylands make small contributions (43.60 ± 25.36 %) (Table S4). Thus, the humid regions are the hotspots with increasing ET and the major contributor to the overall positive land ET trend over the past four decades. These indicate that the humid regions promote "intensified/accelerated" hydrological cycle postulated under global warming from since 1980 s (Jung et al., 2011; Miralles et al., 2014). Meanwhile, these findings suggest a slowing hydrological cycle in drylands (Yang et al., 2019).

3.1.3. *Drylands dominate the IAV in global land ET*

In this overarching positive ET trend in globe, there is a pronounced interannual variability (Fig. 3a). The annual mean ET in humid regions display the long-term increasing ET trend with slight ET IAV, but the drylands exhibit substantial ET IAV (Fig. 3e). Obviously, the times of peak ET in global land overall responds positively to that in drylands, such as the high ET in 1997–1998, 2010, and 2015–2016, and low ET in 1998–2008 and 2019. These above time points precisely correspond to the strong climate events, namely El Niño and La Niña. Anomalies of land precipitation are known to be affected by El Niño/Southern Oscillation (ENSO) events, which also lead to strong anomalies in air temperature and even vegetation dynamics, thereby influencing the ET IAV (Miralles et al., 2014).

Quantitatively, the humid regions only explain 40.34 ± 23.06 % of the total IAV, notwithstanding their large land area and substantial total ET (Fig. 3). The low ET in drylands does not mean that ET is stable in these regions. Although the annual mean ET in drylands accounts for 27.53 ± 2.38 % of that in global land ET (Fig. 3b), the drylands contribute the largest fraction of the IAV in the global land ET, with values being 61.52 % for SiTHv2 model and an average of 59.66 ±

16.89 % for the five ET products (Fig. 3f). The contributions from CMIP6 also vary from 41.11 to 82.09 % (mean value = 61.27 %; Table S5). These results suggest that drylands are critical hotspots controlling the IAV of the global land ET. Previous studies have paid more attention on the role of dryland in carbon cycle (Ahlström et al., 2015; Yao et al., 2020; Barnes et al., 2021), and energy cycle (Zhou et al., 2021), but our results highlight the role of drylands in the hydrological cycle during the recent four decades.

3.2. Attributions of ET IAV over divergent regions

There is a strong positive correlation between the monthly ET IAV and the Southern Oscillation Index (SOI) in Australia, Southern Africa, and high northern latitudes (Fig. 4a). Positive SOI values indicate La Niña conditions, and hence, a positive correlation indicates wetter conditions in the aforementioned regions during La Niña and drier conditions during El Niño. By contrast, the regions with negative ET IAV-SOI correlation, such as Amazonia, Indonesia, Horn of Africa, southern America, and west Asia, occur the opposite conditions. Totally, the monthly ET IAV in dryland and global land derived from various ET models are both positively correlated with the SOI at statistical significance level, with correlations of 0.27 ± 0.05 and 0.11 ± 0.09 (Fig. 4b). However, there is negative correlation between ET IAV and SOI correlation in humid regions.

To investigate whether ENSO events play a role in the ET IAV, soil moisture (SM) and vegetation dynamics (normalized differential vegetation index (NDVI)) relationships, we explore the correlations between monthly IAV of ET, SM and NDVI at grid cells with significant ET IAV-SOI correlations during La Niña and El Niño, respectively (Fig. 4c). In the humid regions, there is no clear relationship between the interannual variability of monthly ET, SM and NDVI during La Niña and El Niño, and ENSO has little or no influence on the relationship (Fig. S8). These results suggest that the large-scale ENSO events in some parts of the humid regions are not accompanied by both increases and decreases in moisture supply and vegetation dynamics, leading to the more complex in ET IAV. In the drylands, regions with significant correlations between ET IAV and SOI largely shows a strong positive ET IAV-SM (R = 0.70; R = 0.73) and ET IAV-NDVI correlations (R = 0.55; R = 0.53)

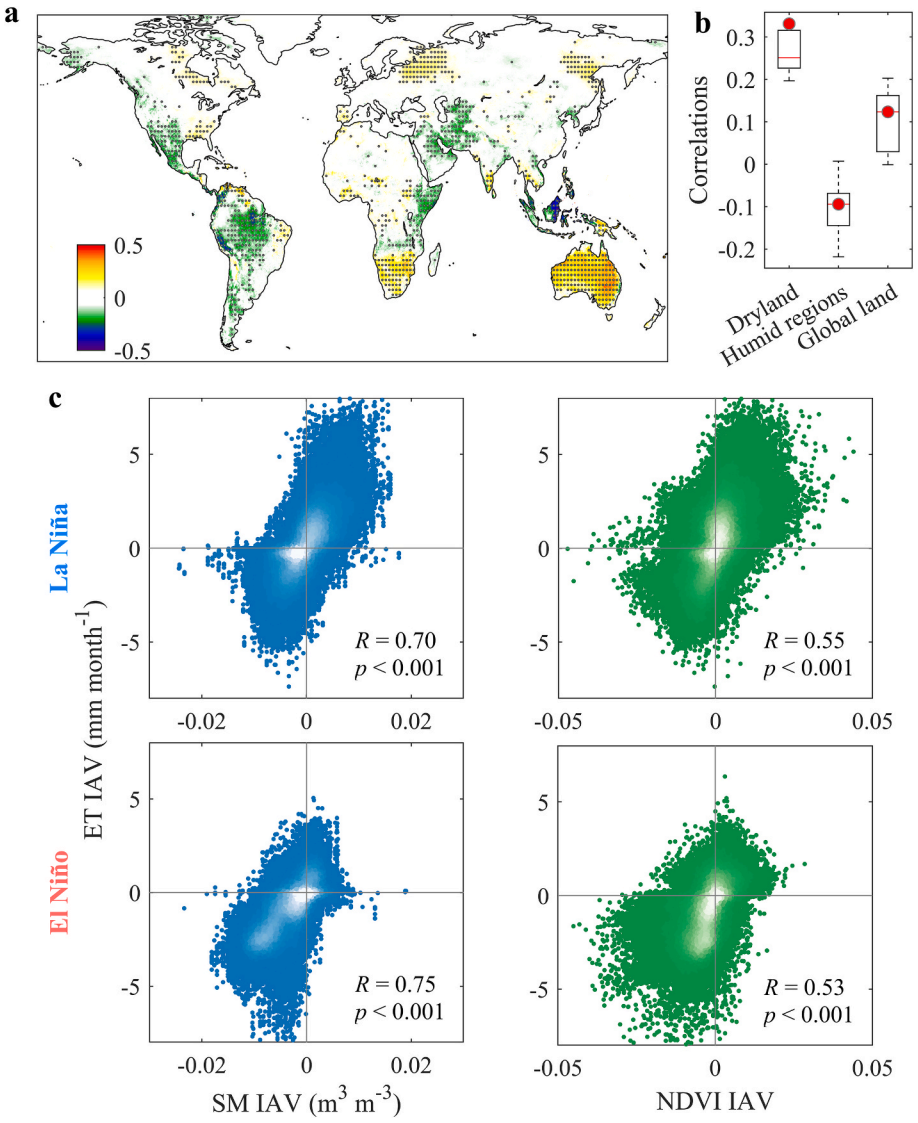

Fig. 4. Causality for interannual variability of ET. (a) Correlation between monthly ET IAV and SOI from 1982 to 2020 at each 0.1° by 0.1° grid cell. Stippling indicates that the correlation is statistically significant ($p < 0.05$). (b) Correlation between ET IAV and SOI grouped by different regions. For each boxplot, the bottom, middle, and top of the box are the 25th, 50th, and 75th percentiles, respectively. (c) Scatterplots of ET IAV versus soil moisture and NDVI for grid cells with statistically significant ET IAV-SOI correlations at during La Niña and (bottom) El Niño, respectively. More details about used SM and NDVI datasets are seen from Text S1.

during La Niña and El Niño events (Fig. 4c). These results indicate that ENSO events have a significant influence on the relationship between ET, SM, and NDVI in drylands. During La Niña, the regions where precipitation increases, appear the sufficient soil moisture and vegetation greening, leading to positive ET anomalies (top plots in Fig. 4c, top right corner); conversely, there are negative ET anomalies (top plots in Fig. 4c, bottom left corner). During the El Niño period, most areas experienced reduced precipitation, resulting in the most grid cells with the decrease in soil moisture and vegetation water stress (bottom plots in Fig. 4c, bottom left corner).

3.3. Attributions of ET trend over divergent regions

3.3.1. The sensitivity of ET to impact factors

The sensitivity of ET to the changes in impact factors is expressed as the partial derivative in the multiple linear regression of the interannual differences in ET against three factors (Zhang et al., 2016). The ET in humid regions show high positive sensitivity to the variation in T_a, especially in the low-mid latitudes regions with high annual mean temperature (Fig. 5a-c, top right corner), such as Amazon basin, Congo basin, and southeast China. At the humid regions, ET in low-mid latitude increases highly with rising temperatures due to abundant moisture (Forzieri et al., 2017; Yang et al., 2023), while the ET in high latitudes has a relative low response to temperature due to the adjustment of permafrost melting and seasonal moisture stress (Zhang et al., 2011, 2020; Liao et al., 2023), resulting in relatively low $\partial ET/\partial T_a$ in high latitudes. On the contrary, the ET in drylands has a negative sensitivity to the T_a changes (Fig. 5a-c, top left corner). Meanwhile, the absolute values of $\partial ET/\partial T_a$ in humid regions is obviously higher than that in drylands across all latitudes (Fig. 5b).

Inversely, ET shows opposite patterns of sensitivity to P compared that with T_a, and the sensitivity of ET to P changes in drylands are obviously stronger than that in humid regions (Fig. 5d-f). Latitudinally, the absolute values of $\partial ET/\partial P$ in drylands is also higher than that in humid regions. In drylands, ET is mainly limited by water supply, and the precipitation that falls on the surface is basically returned to the

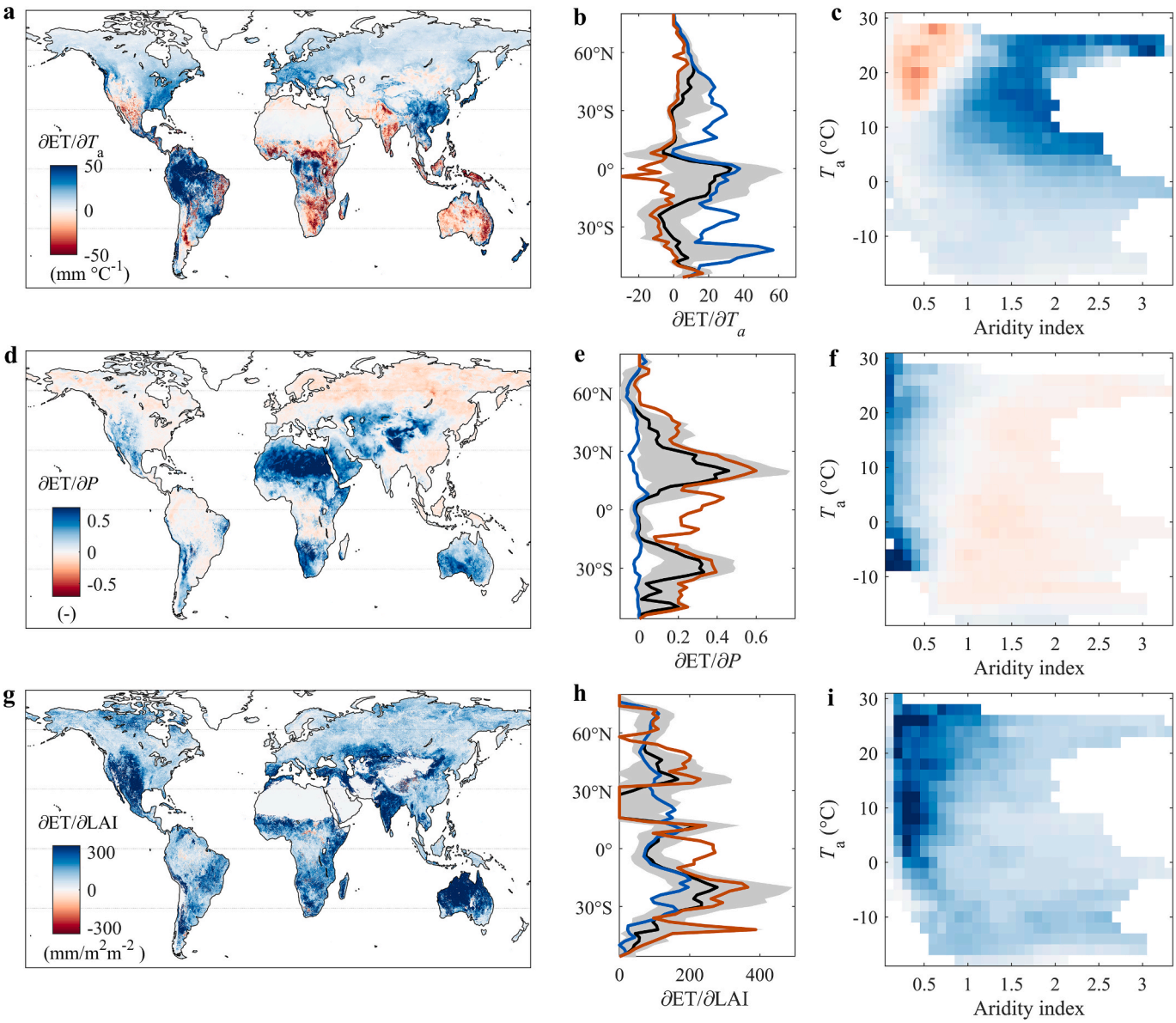

Fig. 5. Sensitivity of ET to multiple drivers. (a) Spatial pattern of sensitivity of ET to T_a. (b) Zonal median of $\partial ET/\partial T_a$ at 5° latitudinal resolution and corresponding interquartile range shown as a black line and gray shaded band, respectively. (c) The $\partial ET/\partial T_a$ binned as a function of climatological medians of Aridity (AI, x axis) and air temperature (T_a, y axis). (d)-(f) and (g)-(i) same as (a) to (c), but for the sensitivity of ET to precipitation ($\partial ET/\partial P$) and LAI ($\partial ET/\partial LAI$), respectively.

atmosphere in the form of soil evaporation and plant transpiration (Yang et al., 2019; Chen et al., 2022). Therefore, the increase/decrease of precipitation directly affect the amount of water distributed to evaporation in drylands, leading to high ∂ET/∂P.

The positive ∂ET/∂LAI nearly occurs on all land surfaces, while the values in drylands are obviously higher than in humid regions (Fig. 5g-i). In these regions, the sensitivity of ET to P and LAI variation shows high consistence in drylands (Forzieri et al., 2020; Yang et al., 2023), due to the stronger coupling of vegetation dynamics with soil moisture driven by precipitation. In fact, high levels of precipitation in drylands lead to moist soils that stimulate vegetation greening, which in turn promotes high rates of ET through transpiration process and soil evaporation, and opposite situations occurs in the low levels of precipitation (Miralles et al., 2014; Forzieri et al., 2017). Furthermore, despite potential limitations of soil moisture on ET due to low rainfall, an increase in LAI can maintain an increase in ET through complex adjustments of vegetation structure and environmental condition, such as root development, access to groundwater and phenological seasonal shifts (Zhu et al., 2023; Behzad, et al., 2023; Gu et al., 2025). However, at local scales in the humid regions, transpiration rate does not continue to increase with the increase in LAI, instead levelling off (or even slightly decreasing) when the LAI exceeds ~ 2; this change emerges due to the canopy has approached the maximum evaporation capacity (that is potential evapotranspiration), and further increase in LAI has a limited contribution to ET (Wang et al., 2019). In addition, LAI has a relatively weak dependence on precipitation (vegetation growth is not limited by water), so the sensitivity of ET to both LAI and precipitation is relatively low.

3.3.2. Warming controls the ET trend in humid regions

The effects of impact factors on ET trend are quantified by multiplying the three sensitivities with trends in LAI, P and T_a, respectively. Indeed, multiple linear regression indicates that these three factors together explain 82.26 % of variations in ensemble mean global ET over 1982–2020. Along with the vegetation greening globally observed by satellites (Chen et al., 2019), increased LAI dominates the ET trend across 34.31 % of global land area over 1982–2020, among which 58.41 % locates in humid regions and 41.59 % in drylands (Fig. 6a-b). Among the three factors, vegetation greening is the largest contributor (Zhang et al., 2015; Piao et al., 2019; Yang et al., 2023), explaining 63.69 ± 25.13 % (or 0.28 ± 0.09 mm year^{-2}; $p < 0.01$) of the global trend over 1982–2020 (Fig. 4). The dominant roles of climate warming in the global land ET trend occurs over 42.84 % of global land area, among which 73.55 % locates in humid regions, accounting for 54.59 ± 17.25 % (or 0.24 ± 0.08 mm year^{-2}; $p < 0.01$) of the global land ET trend. Changes in the P dominate the ET trend across 22.84 % of Earth surface, among which 82.46 % locates in drylands (Zhang et al., 2016), explaining −22.13 ± 17.25 % (or −0.10 ± 0.08 mm year^{-2}; $p < 0.01$) of the global ET trend. In drylands, the positive effect of vegetation greening (0.36 ± 0.12 mm year^{-2}) offsets the negative effects of warming and reduced precipitation ($\delta ET^{Ta} = -0.18 \pm 0.11$ mm year^{-2}; $\delta ET^{P} = -0.21 \pm 0.19$ mm year^{-2}), making the ET trend less obvious. At the humid regions, the positive sensitivities of ET to T_a and LAI in combination with the increasing trends of these factors cause the

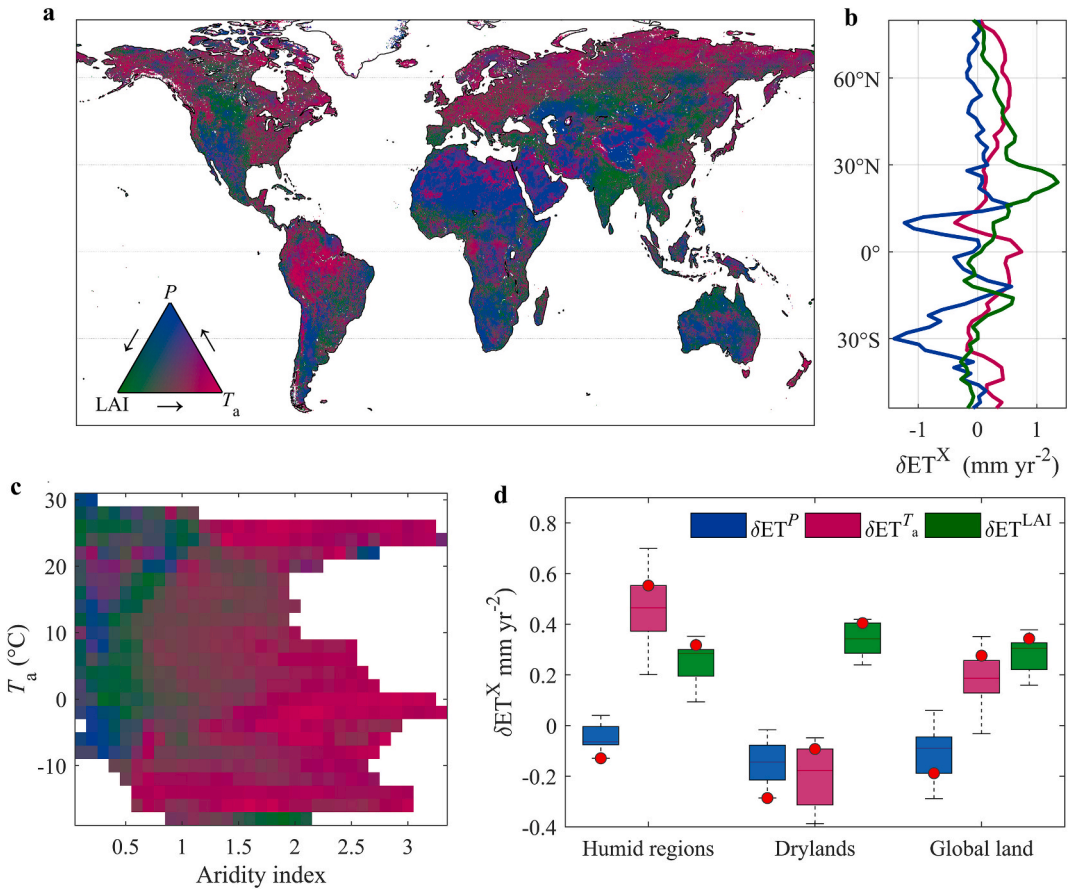

Fig. 6. Primary environmental (air temperature, precipitation and LAI) controls on ET trend over 1982–2020. (a-b) Spatial and latitudinal distribution of primary environmental factors on ET trends. (c) Primary environmental (air temperature, precipitation and LAI) controls on ET trend binned as a function of climatological medians of aridity index (x axis) and air temperature (T_a, y axis). (d) Effects (x) of the long-term trends in LAI, T_a, and P on the ET (δET^x). For each boxplot, the bottom, middle, and top of the box are the 25th, 50th, and 75th percentiles, respectively, and the bottom and top whiskers show the 10th and 90th percentiles, respectively.

positive ET trend (δET^{Ta} = 0.43 ± 0.2 and δET^{LAI} = 0.30 ± 0.13 mm year^{-2}), which subsequently drives the global land ET upward trend. Thus, our results confirm that the main contributions of the intensified or accelerated water cycle (Huntington et al., 2006; Madakumbura et al., 2019) are from the humid regions mainly due to global warming (increased T_a and R_n) and plant greening.

In humid regions, the ET mainly controlled by the atmospheric moisture demand (air temperature) and vegetation dynamic (LAI) (Fig. 7). The increase in ET mainly locates in the humid regions in the Northern Hemisphere, accounting for 83.32 ± 13.77 % of increase in global land. Seasonally, the ET in summer contributes the largest fraction (40.73 ± 8.93 %) to the increase in global land, followed by autumn (24.29 ± 2.48 %), spring (22.12 ± 5.98 %), and winter (11.56 ± 9.56 %). In this domain, the warming and vegetation greening control the increase in ET. Firstly, the advanced onset of the growing season and earlier spring thaw associated with warming, have produce sufficient soil moisture (Fig. 7b-c) to satisfy strong atmospheric moisture demand, which is often associated with the high temperature, and then make photosynthesis (transpiration) rapidly recover and proceed at relatively high rates with enough moisture supply (Fig. 7c-d) (Menzel et al., 2006; Fu et al., 2016; Pi et al., 2021). In addition, the accumulated soil moisture in spring also supplies the adequate moisture for strong photosynthesis in summer (Fig. 7e and h). Meanwhile, the delayed end time of growing season and later autumn freeze-up, lead to the relatively adequate soil moisture to sustain plant activities. The warming boosted vegetation growth in high latitudes (Park et al., 2020; Piao et al., 2014, 2017), which lead to the continuous greening (Fig. 7g-i) and positive effect of LAI on ET. In turn, the increased LAI can enhance the warming in this domain through a decline of surface albedo (Forzieri et al., 2017; Jeong et al., 2012; Swann et al., 2010; Liao et al., 2023; Li et al., 2024a). In the future, the ET in humid regions will potentially continue to increase with the expectation of global warming and vegetation greening, but it largely depends on how vegetation adapts to water stress under drought (Zhang et al., 2011; Li et al., 2024b).

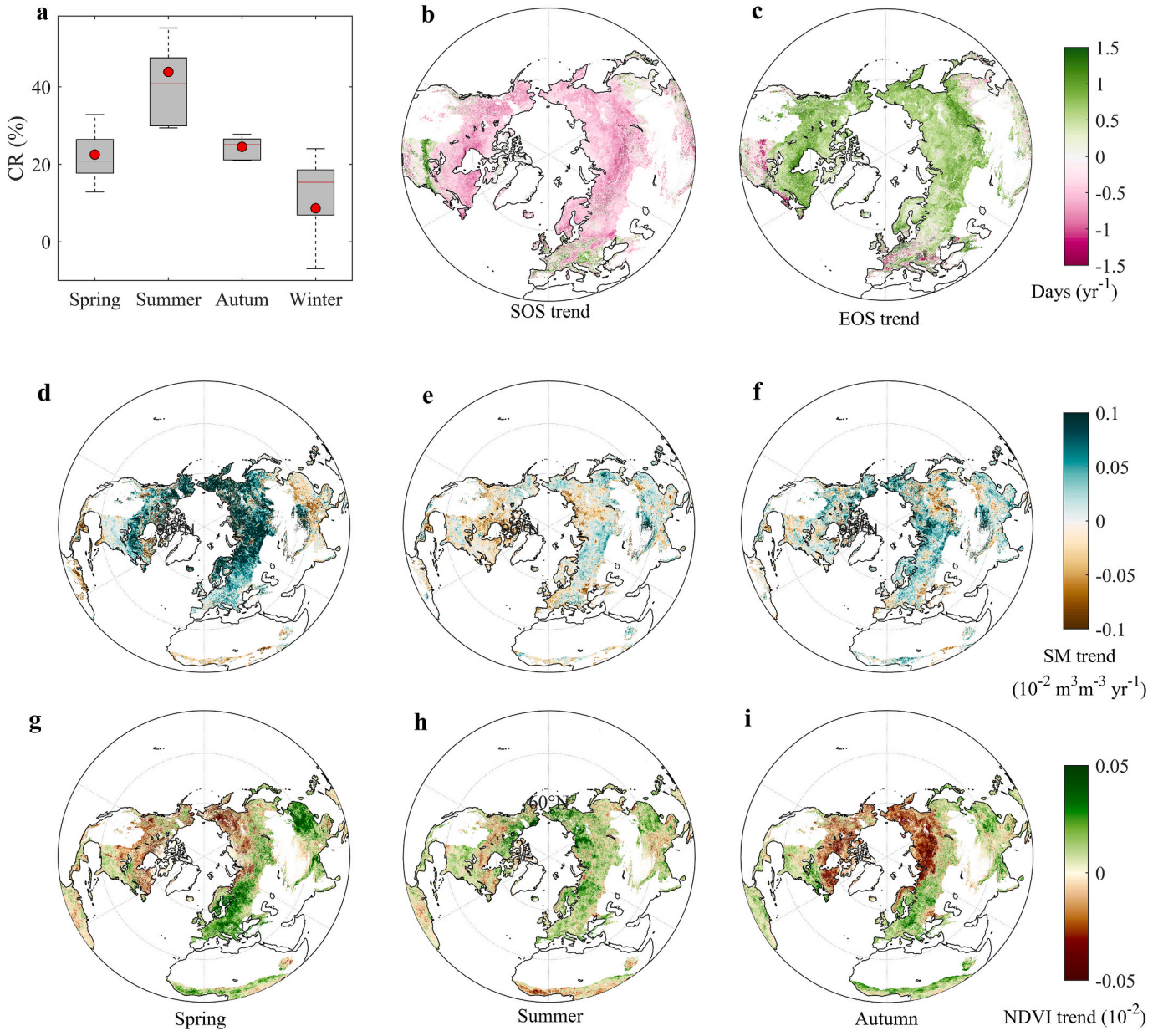

Fig. 7. Changes in the seasonality of ET trend and the linkage with changes in vegetation phenology, soil moisture and NDVI in humid regions. (a) Contributions of seasonal ET in humid regions. (b)-(c) The trend in the start of growing season (SOS) and end of growing season (EOS). (d)-(f) The trend in seasonal soil moisture. (g)-(i) The trend in seasonal NDVI. More details about used SM and NDVI datasets are seen in Text S1.

3.4. Future ET dynamics

In addition to observed changes since approximately 1980, ET is anticipated to evolve in the future according to CMIP6 ESMs. Although there will still be significant interannual fluctuations in global ET in the future, global ET as a whole still shows an upward trend regardless of the climate change scenarios (Fig. S9). For example, over 2015–2100, CMIP6 ESMs project an increasing global ET trend of 0.36 ± 0.25, 0.42 ± 0.29, and 0.56 ± 0.40 mm year^{-2} for Shared Socio-economic Pathway (SSP)1–2.6, SSP3–7.0 and SSP5–8.5, respectively (Fig. S9). Consistent with the historical period, future ET trends in global land are still primarily dominated by the humid regions (Fig. 8a-c and d). Nevertheless, the contributions of future ET in humid regions generally deceases with increasing emission levels, possibly owing to larger stomatal closure under water stress (Zhang et al., 2021; Yang et al., 2023; Chai et al., 2025). However, the projected contributions in humid regions are still higher than that for the historical period from CMIP6 models, and smaller than that from diagnostic ET datasets (Fig. 8b and Fig. 4b). In addition, the changing rates in most land areas increase with increasing emission levels (Fig. 8a), indicating the accelerated hydrology cycle. Continuous increase in ET in humid regions may maintain or strengthen the positive feedback of precipitation-evaporation, and also mitigate climate warming through the evaporation cooling effect and increased albedo through cloud formation, thereby influencing climate change (Mondal et al., 2024; Hofmann et al., 2023; Gao et al., 2025; Teuling, et al., 2013; Leggett and Ball, 2019). For a given precipitation, an increase in ET would elevate the evaporation ratio (i.e., ET/*P*), consequently resulting in a long-term decline in available water resources. However, variations in ET and vegetation change will further change regional precipitation via land-atmospheric interactions,

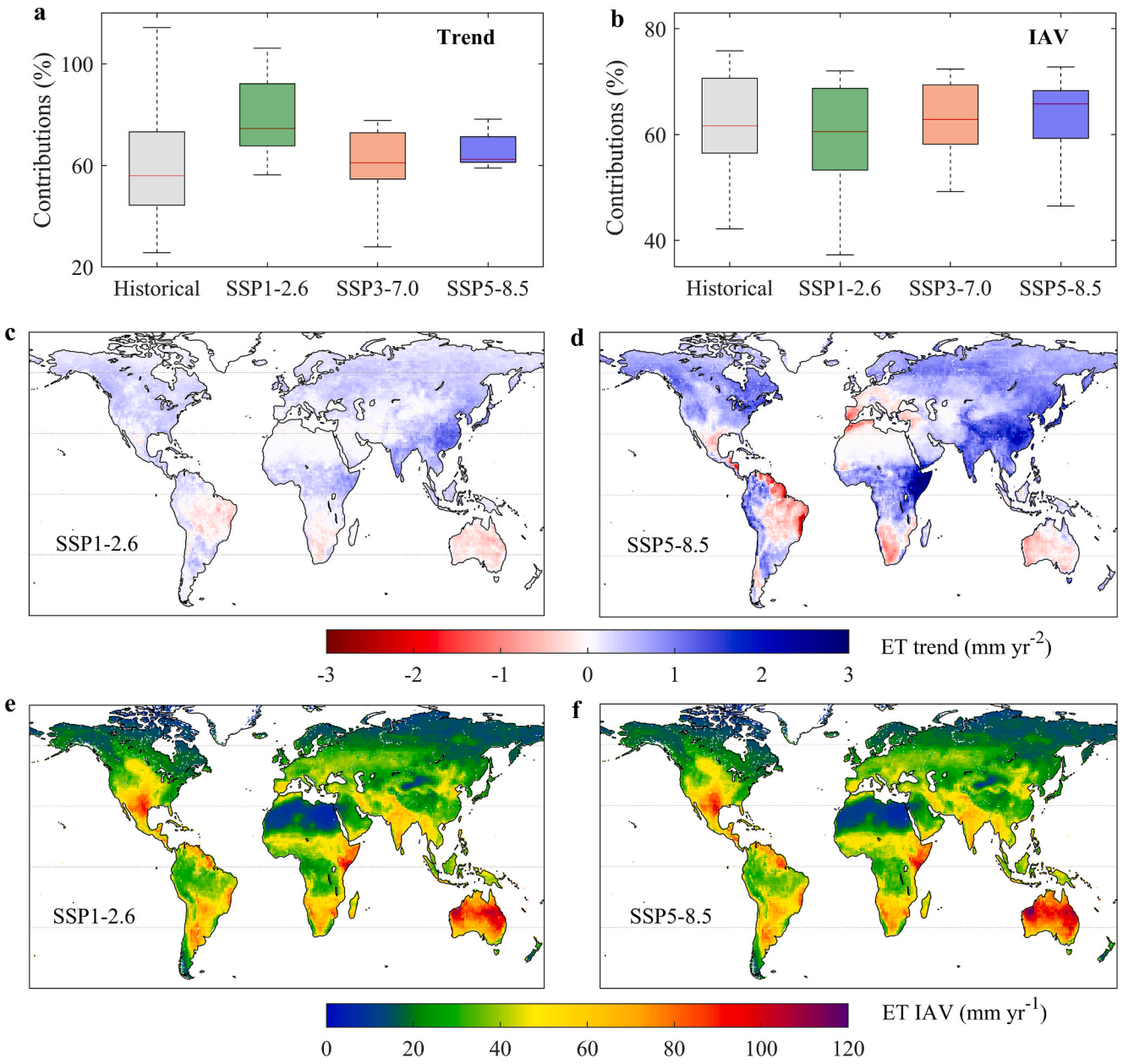

Fig. 8. Projected changes in global land evapotranspiration. (a) Comparison of contributions of humid regions ET to global land ET trend in CMIP6 models under different scenarios. (b) Comparison of contributions of drylands ET to global land ET IAV in CMIP6 models under different scenarios. (c) – (d) Future (2015–2100) ET trend under the climate change scenario SSP1-2.6 and SSP-8.5. (e) – (f) Future (2015–2100) ET IAV under the climate change scenario SSP1-2.6 and SSP-8.5. The projected changes in ET from 10 CMIP6 ESMs can be seen from Table S6.

thereby influencing the changes in available water resources (Konapala et al., 2020; Zhang et al., 2023). Moreover, more ET means more transpiration, and then more carbon can be assimilated by plant photosynthetic activity. With more carbon fixed, more leaves and plants can grow, subsequently resulting in more water consumed by transpiration in return (Gentine et al., 2019; Papanatsiou et al., 2019; Joshi et al., 2022). With the increasing CO_2 concentration, the humid regions (such as tropical rainforest and some mid-to-high latitude forests) may experience "greening" and an increase in productivity, as the warming and CO_2 fertilization effects can promote plant growth when water supply is not limited (Piao et al., 2019; Allen et al., 2024). However, this growth may be accompanied by changes in vegetation types (such as the advance of temperate broadleaf forests towards the north) (Ashton et al., 2020; Wang et al., 2024). In the future, combining with the global change, the complex coupling processes among water, energy, and carbon should be taken into consideration when investigating the impacts of ET changes in humid regions.

The IAV of ET in drylands remains the dominant driver of the future global ET IAV. Meanwhile, the contribution factions of future ET IAV in drylands generally increase with increasing emission levels (Fig. 8b). Accordingly, the projected contributions in drylands are higher than that for the historical period from CMIP6 models and diagnostic ET data sets (Fig. 4b). Because drylands are the most sensitive areas responding to global change, with the intensify and frequent extreme events in drylands in the future (Camps-Valls et al., 2025; Li et al., 2024), these lead to stronger climate variability, thereby resulting in the huge ET IAV. In the future, even small shifts in the precipitation-runoff-evaporation relationship will be amplified into significant fluctuations in runoff and water resources in dryland, reducing the predictability of water resources (Berghuijs et al., 2017). Evaporation demand is rising with global warming, erratic rainfall reduces recharge, leading to severe water stress, aquifer depletion, drying lakes, reduced river flows, and escalating conflicts over shared river resources in drylands (IPCC, 2023). Moreover, due to the stronger land–atmosphere water coupling in drylands (Seneviratne et al., 2010), the greater ET IAV will in turn enhance drylands climate change and extreme climate events under increasing emission levels (Zhao et al., 2022; Vicente-Serrano et al., 2025; He et al., 2025). The expansion of drylands and the increase in drought intensity will lead to an increase in the frequency and duration of extreme droughts, causing devastating impacts on agriculture, ecology and urban water supply, causing the chain reaction of hydrological extreme events (Tang et al., 2025). In the context of above, the vulnerability of the ecological environment in drylands will strengthen, so more attentions should be focused on the future hydrological cycle in drylands, to improve water management and design adaptation policies.

However, large uncertainties exist in current understanding of global land ET (Mirallers et al., 2025; Yang et al., 2023). The ET trends and IAV derived from individual estimates still remains discrepancies, especially at regional and/or local scales (Figs. 1–3). These differences mainly arise from different model structures, parameterizations, and forcing datasets among the ET models. For example, there are different structures of the ET model mainly lying in aspects such as plant root uptake water, soil water movement, stomatal conductance schemes, and root distribution (Chen et al., 2022; Mirallers et al., 2025; Fisher et al., 2017). The uncertainty in ET trends and IAVs highlights a need for caution in using a single approach to analyze long-term ET changes. Using the models ensemble mean can reduce the uncertainty of the results, but we still develop more advanced multi-model ensemble techniques (such as bias correction, model weighting, and model-data fusion technology) may also help reduce the uncertainties (Yang et al., 2023). Additionally, conducting a comprehensive comparison of evaporation models driven by the same forcing data can help identify the sources of uncertainty, thereby providing practical guidance for improving ET estimation.

4. Conclusion

Our study finds that regions driving the overall trend and IAV of the global land ET are divergent, providing us with a crucial framework for understanding the dynamics of land ET over the past four decades. The process-based models combing with remote-sensing observations provides us an effective strategy to investigate the spatio-temporal changes in land ET and the relative contributions of the climatic and ecological factors. The remote-sensing observations can greatly reduce uncertainties of some process simulations, such as CO_2 fertilization effects on vegetation products. To conclude, the humid regions drive the increase in the global land ET, which is mostly explained by global warming and vegetation greening. On the other hand, the drylands dominated IAV of the global land ET due to the natural climate variability (ENSO). Importantly, the dominant roles of humid regions and drylands in global land ET trend and IAV will continue under the climate change scenarios. Most current models may underestimate the nonlinear response of ET in drylands to extreme climate events, while overestimating the stability of humid regions under long-term climate change. Our findings provide a new perspective for understanding the spatial heterogeneity of the global water-carbon coupling cycle. Meanwhile, our results suggest that land surface model should differentiate in handling the biophysical parameterization schemes for different climate zones, and particularly, strengthen the dynamic characterization of the groundwater-soil–vegetation–atmosphere continuum (GSPAC) process in drylands to improve the accuracy of global hydrological flux predictions. The ET change in humid regions profoundly restructure the global precipitation pattern, alters the warming rate, and influences the ecohydrology process, such as the water resources and carbon cycle. Due to the roles of climate and vegetation changes in the dynamics of ET in humid regions, under the context of the global warming, the ET changes mostly determined by the adaptability of plant growth to water stress, suggesting that more concerns should paid on the interactions between ecological processes and hydrological cycle. In drylands, the stronger ET IAV can increase the frequency of extreme climate events, give rise to the expansion of drylands areas, and leading to a more fragile ecological environment. It is necessary to pay attention to the hydrological cycles in global drylands should aid in improving water management and designing adaptation policies. Furthermore, the global impact of humid regions combining with the fluctuation of ET in arid regions, jointly amplify the complexity of the climate system. In the future, it is necessary to focus on the interaction between humid and arid regions, in order to achieve collaborative governance of global hydrological and ecological risks.

CRediT authorship contribution statement

Huiling Chen: Writing – review & editing, Writing – original draft. **Kun Zhang:** Writing – review & editing. **Gaofeng Zhu:** Writing – review & editing, Funding acquisition, Conceptualization. **Lei Fan:** Writing – review & editing. **Xin Li:** Writing – review & editing. **Yunquan Wang:** Writing – review & editing, Methodology, Conceptualization. **Xufeng Wang:** Writing – review & editing, Conceptualization. **Shasha Shang:** Software, Resources, Methodology. **Jia Jia:** Methodology. **Yongtai Zhu:** Validation, Methodology. **Jingfeng Xiao:** Writing – review & editing.

Declaration of competing interest

The authors declare that they have no known competing financial interests or personal relationships that could have appeared to influence the work reported in this paper.

Acknowledgements

This research was supported by the National Natural Science Foundation of China (grant nos. 42471105, 42571409, and 42171019), the

Natural Science Foundation of Gansu Province (23JRRA1025), and the Natural Science Foundation of ZheJiang Province (LQN26D010006). We thank all the PIs and other research personnel contributed to this study.

Appendix A. Supplementary data

Supplementary data to this article can be found online at https://doi.org/10.1016/j.jhydrol.2025.134879.

Data availability

MTE is available at http://www.bgc-jena.mpg.de/geodb/; ERA5-Land download from https://cds.climate.copernicus.eu/cdsapp#!/dataset/reanalysis-era5-land?tab = form; Noah_GL is from https://disc.gsfc.nasa.gov/datasets/GLDAS_NOAH025_3H_2.1/su mmary; GLEAM product is the latest version of GLEAM v4.2a datasets developed by Miralles et al. (2025); CR dataset is available from Doi: 10.6084/m9.figshare.13634552. The CMIP6 model simulations are publicly available from https://aims2.llnl.gov/search/?project=CMIP6.

References

Aguilos, M., Sun, G., Liu, N., Zhang, Y., Starr, G., Oishi, A.C., O'Halloran, T.L., Forsythe, J., Wang, J., Zhu, M., Amatya, D., Baniya, B., McNulty, S., Noormets, A., King, J., 2024. Energy availability and leaf area dominate control of ecosystem evapotranspiration in the southeastern U.S. Agric. For. Meteorol. 349, 109960. https://doi.org/10.1016/j.agrformet.2024.109960.

Ahlström, A., Raupach, M.R., Schurgers, G., Smith, B., Arneth, A., Jung, M., Reichstein, M., Canadell, J.G., Friedlingstein, P., Jain, A.K., Kato, E., Poulter, B., Sitch, S., Stocker, B.D., Viovy, N., Wang, Y.P., Wiltshire, A., Zaehle, S., Zeng, N., 2015. The dominant role of semi-arid ecosystems in the trend and variability of the land CO_2 sink. Science 348, 895–899. https://doi.org/10.1126/science.aaa1668.

Allan, R.P., Barlow, M., Byrne, M.P., Cherchi, A., Douville, H., Fowler, H.J., Gan, T.Y., Pendergrass, A.G., Rosenfeld, D., Swann, A.L.S., Wilcox, L.J., Zolina, O., 2020. Advances in understanding large-scale responses of the water cycle to climate change. Ann. N. Y. Acad. Sci. 1472, 49–75. https://doi.org/10.1111/nyas.14337.

Allen, R.J., Gomez, J., Horowitz, L.W., Shevliakova, E., 2024. Enhanced future vegetation growth with elevated carbon dioxide concentrations could increase fire activity. Commun. Earth Environ. 5, 54. https://doi.org/10.1038/s43247-024-01228-7.

Ashton, P., Zhu, H., 2020. The tropical-subtropical evergreen forest transition in East Asia: an exploration. Plant Divers. 42, 255–280. https://doi.org/10.1016/j.pld.2020.04.001.

Beaudoing, H., Rodell, M., 2019. GLDAS Noah land surface model L4 monthly 0.25 × 0.25degree V2.0. Greenbelt. Goddard Earth Sciences Data and Information Services Center (GES DISC). Doi: 10.5067/9SQ1B3ZXP2C5.

Barnes, M.L., Farella, M.M., Scott, R.L., Moore, D.J., Ponce-Campos, G.E., Biederman, J. A., MacBean, N., Litvak, M.E., Breshears, D., 2021. Improved dryland carbon flux predictions with explicit consideration of water-carbon coupling. Commun. Earth & Environ. 2, 248. https://doi.org/10.1038/s43247-021-00308-2.

Beck, H.E., Dijk, A.I.J.M. van, Larraondo, P.R., McVicar, T.R., Pan, M., Dutra, E., Miralles, D.G., 2022. MSWX: Global 3-Hourly 0.1° Bias-Corrected Meteorological Data Including Near-Real-Time Updates and Forecast Ensembles. Doi: 10.1175/BAMS-D-21-0145.1.

Beck, H.E., Wood, E.F., Pan, M., Fisher, C.K., Miralles, D.G., Van Dijk, A.I., McVicar, T.R., Adler, R.F., 2019. MSWEP V2 global 3-hourly 0.1 precipitation: methodology and quantitative assessment. Bull. Am. Meteorol. Soc. 100, 473–500. https://doi.org/10.1175/BAMS-D-17-0138.1.

Behzad, H.M., Arif, M., Duan, S., Kavousi, A., Cao, M., Liu, J., Jiang, Y., 2023. Seasonal variations in water uptake and transpiration for plants in a karst critical zone in China. Sci. Total Environ. 860, 160424. https://doi.org/10.1016/j.scitotenv.2022.160424.

Berghuijs, W.R., Larsen, J.R., van Emmerik, T.H.M., Woods, R.A., 2017. A global assessment of runoff sensitivity to changes in precipitation, potential evaporation, and other factors. Water Resour. Res. 53, 8475–8486. https://doi.org/10.1002/2017WR021593.

Camps-Valls, G., Fernández-Torres, M.Á., Cohrs, K.H., Höhl, A., Castelletti, A., Pacal, A., Robin, C., Martinuzzi, F., Papoutsis, I., Prapas, I., Pérez-Aracil, J., Weigel, K., Gonzalez-Calabuig, M., Reichstein, M., Rabel, M., Giuliani, M., Mahecha, M.D., Popescu, O.I., Pellicer-Valero, O.J., Ouala, S., Salcedo-Sanz, S., Sippel, S., Kondylatos, S., Happé, T., Williams, T., 2025. Artificial intelligence for modeling and understanding extreme weather and climate events. Nat. Commun. 16. https://doi.org/10.1038/s41467-025-56573-8.

Cao, S., Li, M., Zhu, Z., Wang, Z., Zha, J., Zhao, W., Duanmu, Z., Chen, J., Zheng, Y., Chen, Y., Myneni, R.B., Piao, S., 2023. Spatiotemporally consistent global dataset of the GIMMS leaf area index (GIMMS LAI4g) from 1982 to 2020. Earth Syst. Sci. Data 15, 4877–4899. https://doi.org/10.5194/essd-15-4877-2023.

Chai, Y., Miao, C., Slater, L., Ciais, P., Berghuijs, W.R., Chen, T., Huntingford, C., 2025. Underestimating global land greening: Future vegetation changes and their impacts on terrestrial water loss. One Earth 8 (2). https://www.cell.com/one-earth/abstract/S2590-3322(25)00002-8.

Chen, C., Park, T., Wang, X., Piao, S., Xu, B., Chaturvedi, R.K., Fuchs, R., Brovkin, V., Ciais, P., Fensholt, R., Tømmervik, H., Bala, G., Zhu, Z., Nemani, R.R., Myneni, R.B., 2019. China and India lead in greening of the world through land-use management. Nat. Sustain. 2, 122–129. https://doi.org/10.1038/s41893-019-0220-7.

Chen, H., Zhu, G., Shang, S., Qin, W., Zhang, Y., Su, Y., Zhang, K., Zhu, Y., Xu, C., 2022. Uncertainties in partitioning evapotranspiration by two remote sensing-based models. J. Hydrol. 604, 127223. https://doi.org/10.1016/j.jhydrol.2021.127223.

Chen, H., Zhu, G., Zhang, K., Bi, J., Jia, X., Ding, B., Zhang, Y., Shang, S., Zhao, N., Qin, W., 2020. Evaluation of evapotranspiration models using different LAI and meteorological forcing data from 1982 to 2017. Remote Sens. (Basel) 12, 2473. https://doi.org/10.3390/rs12152473.

Condon, L.E., Atchley, A.L., Maxwell, R.M., 2020. Evapotranspiration depletes groundwater under warming over the contiguous United States. Nat. Commun. 11. https://doi.org/10.1038/s41467-020-14688-0.

Dorigo, W., Dietrich, S., Aires, F., Brocca, L., Carter, S., Cretaux, J.-F., Dunkerley, D., Enomoto, H., Forsberg, R., Güntner, A., Hegglin, M.I., Hollmann, R., Hurst, D.F., Johannessen, J.A., Kummerow, C., Lee, T., Luojus, K., Looser, U., Miralles, D.G., Pellet, V., Recknagel, T., Vargas, C.R., Schneider, U., Schoeneich, P., Schröder, M., Tapper, N., Vuglinsky, V., Wagner, W., Yu, L., Zappa, L., Zemp, M., Aich, V., 2021. Closing the water cycle from observations across scales: where do we stand? Bull. Am. Meteorol. Soc. 102, E1897–E1935. https://doi.org/10.1175/bams-d-19-0316.1.

Douville, H., Ribes, A., Decharme, B., Alkama, R., Sheffield, J., 2013. Anthropogenic influence on multidecadal changes in reconstructed global evapotranspiration. Nat. Clim. Change 3, 59–62. https://doi.org/10.1038/nclimate1632.

Egli, M., Humphrey, V., Sippel, S., Knutti, R., 2024. A distinct role for aerosol and GHG forcing in historical CMIP6 evapotranspiration trends. Earth's Future 12. https://doi.org/10.1029/2024ef004973.

Eyring, V., Bony, S., Meehl, G.A., Senior, C.A., Stevens, B., Stouffer, R.J., Taylor, K.E., 2016. Overview of the coupled model intercomparison project phase 6 (CMIP6) experimental design and organization. Geosci. Model Dev. 9, 1937–1958. https://doi.org/10.5194/gmd-9-1937-2016.

Fisher, J.B., Melton, F., Middleton, E., Hain, C., Anderson, M., Allen, R., McCabe, M.F., Hook, S., Baldocchi, D., Townsend, P.A., Kilic, A., Tu, K., Miralles, D.D., Perret, J., Lagouarde, J., Waliser, D., Purdy, A.J., French, A., Schimel, D., Famiglietti, J.S., Stephens, G., Wood, E.F., 2017. The future of evapotranspiration: Global requirements for ecosystem functioning, carbon and climate feedbacks, agricultural management, and water resources. Water Resour. Res. 53, 2618–2626. https://doi.org/10.1002/2016wr020175.

Forzieri, G., Alkama, R., Miralles, D.G., Cescatti, A., 2017. Satellites reveal contrasting responses of regional climate to the widespread greening of Earth. Science 356, 1180–1184. https://doi.org/10.1126/science.aal1727.

Forzieri, G., Miralles, D.G., Ciais, P., Alkama, R., Ryu, Y., Duveiller, G., Zhang, K., Robertson, E., Kautz, M., Martens, B., Jiang, C., Arneth, A., Georgievski, G., Li, W., Ceccherini, G., Anthoni, P., Lawrence, P., Wiltshire, A., Pongratz, J., Piao, S., Sitch, S., Goll, D.S., Arora, V.K., Lienert, S., Lombardozzi, D., Kato, E., Nabel, J.E.M. S., Tian, H., Friedlingstein, P., Cescatti, A., 2020. Increased control of vegetation on global terrestrial energy fluxes. Nat. Clim. Chang. 10, 356–362. https://doi.org/10.1038/s41558-020-0717-0.

Fu, Y.H., Liu, Y., De Boeck, H.J., Menzel, A., Nijs, I., Peaucelle, M., Peñuelas, J., Piao, S., Janssens, I.A., 2016. Three times greater weight of daytime than of night-time temperature on leaf unfolding phenology in temperate trees. New Phytol. 212, 590–597. https://doi.org/10.1111/nph.14073.

Gao, C., Fu, J., Han, Z., Ji, W., Zhao, L., Wei, X., Li, Z., 2025. Local and downwind precipitation has been boosted by evapotranspiration change-induced moisture recycling in the Chinese Loess Plateau. Agric. For. Meteorol. 371, 110623. https://doi.org/10.1016/j.agrformet.2025.110623.

Gentine, P., Green, J.K., Guérin, M., Humphrey, V., Seneviratne, S.I., Zhang, Y., Zhou, S., 2019. Coupling between the terrestrial carbon and water cycles—a review. Environ. Res. Lett. 14 (8), 083003. https://doi.org/10.1126/science.aaw0046.

Graveline, V., Helbig, M., Gosselin, G.H., Alcock, H., Detto, M., Walker, B., Marsh, P., Sonnentag, O., 2024. Surface-atmosphere energy exchanges and their effects on surface climate and atmospheric boundary layer characteristics in the forest-tundra ecotone in northwestern Canada. Agric. For. Meteorol. 350, 109996. https://doi.org/10.1016/j.agrformet.2024.109996.

Gu, H., Chen, G., Ren, H., Liu, B., Yang, Q., Feng, X., Fan, M., Zhou, H., 2025. Seasonal dynamics of water-use strategies and response to precipitation in different habitats of Nitraria L. J. Hydrol. 648, 132388. https://doi.org/10.1016/j.jhydrol.2024.132388.

He, Q., Wang, M., Liu, K., Wang, B., 2025. High-resolution Standardized Precipitation Evapotranspiration Index (SPEI) reveals trends in drought and vegetation water availability in China. Geogr. Sustain. 6, 100228. https://doi.org/10.1016/j.geosus.2024.08.007.

Hofmann, G.S., Silva, R.C., Weber, E.J., Barbosa, A.A., Oliveira, L.F.B., Alves, R.J.V., Hasenack, H., Schossler, V., Aquino, F.E., Cardoso, M.F., 2023. Changes in atmospheric circulation and evapotranspiration are reducing rainfall in the Brazilian Cerrado. Sci. Rep. 13. https://doi.org/10.1038/s41598-023-38174-x.

Huntington, T.G., 2006. Evidence for intensification of the global water cycle: review and synthesis. J. Hydrol. 319, 83–95. https://doi.org/10.1016/j.jhydrol.2005.07.003.

IPCC, 2023. Climate Change 2023: Synthesis Report. Contribution of Working Groups I, II and III to the Sixth Assessment Report of the Intergovernmental Panel on Climate Change [Core Writing Team, H. Lee and J. Romero (eds.)]. IPCC, Geneva, Switzerland, pp. 35-115. Doi: 10.59327/IPCC/AR6-9789291691647.

Jeong, J.-H., Kug, J.-S., Kim, B.-M., Min, S.-K., Linderholm, H.W., Ho, C.-H., Rayner, D., Chen, D., Jun, S.-Y., 2012. Greening in the circumpolar high-latitude may amplify

warming in the growing season. Clim. Dyn. 38, 1421–1431. https://doi.org/10.1007/s00382-011-1142-x.
Joshi, J., Stocker, B.D., Hofhansl, F., Zhou, S., Dieckmann, U., Prentice, I.C., 2022. Towards a unified theory of plant photosynthesis and hydraulics. Nat. Plants 8 (11), 1304–1316. https://doi.org/10.1038/s41477-022-01244-5.
Jung, M., Reichstein, M., Ciais, P., Seneviratne, S.I., Sheffield, J., Goulden, M.L., Bonan, G., Cescatti, A., Chen, J., De Jeu, R., Dolman, A.J., Eugster, W., Gerten, D., Gianelle, D., Gobron, N., Heinke, J., Kimball, J., Law, B.E., Montagnani, L., Mu, Q., Mueller, B., Oleson, K., Papale, D., Richardson, A.D., Roupsard, O., Running, S., Tomelleri, E., Viovy, N., Weber, U., Williams, C., Wood, E., Zaehle, S., Zhang, K., 2010. Recent decline in the global land evapotranspiration trend due to limited moisture supply. Nature 467, 951–954. https://doi.org/10.1038/nature09396.
Konapala, G., Mishra, A.K., Wada, Y., Mann, M.E., 2020. Climate change will affect global water availability through compounding changes in seasonal precipitation and evaporation. Nat. Commun. 11, 3044. https://doi.org/10.1038/s41467-020-16757-w.
Leggett, L.M.W., Ball, D.A., 2019. Evidence that global evapotranspiration makes a substantial contribution to the global atmospheric temperature slowdown. Theor. Appl. Climatol. 135, 649–675. https://doi.org/10.1007/s00704-018-2387-7.
Li, J., Zhang, Y., Bevacqua, E., Zscheischler, J., Keenan, T.F., Lian, X., Zhou, S., Zhang, H., He, M., Piao, S., 2024a. Future increase in compound soil drought-heat extremes exacerbated by vegetation greening. Nat. Commun. 15, 10875. https://doi.org/10.1038/s41467-024-55175-0.
Li, X., Peng, X., Sun, H., Frauenfeld, O.W., Chen, G., Huang, Y., Wei, G., Du, J., 2024b. The biogeophysical impacts of land cover changes in Northern Hemisphere permafrost regions. Catena 243, 108209. https://doi.org/10.1016/j.catena.2024.108209.
Liao, J., Hang, J., Luo, Q., Luo, H., Ma, T., Wei, Z., Yuan, H., 2023. Seasonal variability of forest cooling and warming effects and response to drought in mid-to-high latitudes of the Northern Hemisphere. For. Ecol. Manage. 546, 121324. https://doi.org/10.1016/j.foreco.2023.121324.
Liu, G., Wang, W., 2025. Competing effects of vegetation greening-induced changes in summer evapotranspiration and precipitation on water yield in the Yangtze River Basin based on WRF simulations. Water Resour. Res. 61. https://doi.org/10.1029/2024wr038663.
Ma, N., Szilagyi, J., Zhang, Y., 2021. Calibration-free complementary relationship estimates terrestrial evapotranspiration globally. Water Resour. Res. 57. https://doi.org/10.1029/2021wr029691.
Ma, N., Zhang, Y., Szilagyi, J., 2024. Water-balance-based evapotranspiration for 56 large river basins: a benchmarking dataset for global terrestrial evapotranspiration modeling. J. Hydrol. 630, 130607. https://doi.org/10.1016/j.jhydrol.2024.130607.
Madakumbura, G.D., Kim, H., Utsumi, N., Shiogama, H., Fischer, E.M., Seland, Ø., Scinocca, J.F., Mitchell, D.M., Hirabayashi, Y., Oki, T., 2019. Event-to-event intensification of the hydrologic cycle from 1.5 °C to a 2 °C warmer world. Sci. Rep. 9. Doi: 10.1038/s41598-019-39936-2.
Menzel, A., Sparks, T.H., Estrella, N., Koch, E., Aasa, A., Ahas, R., Alm-Kübler, K., Bissolli, P., Braslavská, O., Briede, A., Chmielewski, F.M., Crepinsek, Z., Curnel, Y., Dahl, Å., Defila, C., Donnelly, A., Filella, Y., Jatczak, K., Måge, F., Mestre, A., Nordli, Ø., Peñuelas, J., Pirinen, P., Remišová, V., Scheifinger, H., Striz, M., Susnik, A., Van Vliet, A.J.H., Wielgolaski, F., Zach, S., Zust, A., 2006. European phenological response to climate change matches the warming pattern. Glob. Chang. Biol. 12, 1969–1976. https://doi.org/10.1111/j.1365-2486.2006.01193.x.
Miralles, D.G., Bonte, O., Koppa, A., Baez-Villanueva, O.M., Tronquo, E., Zhong, F., Beck, H.E., Hulsman, P., Dorigo, W., Verhoest, N.E.C., Haghdoost, S., 2025. GLEAM4: global land evaporation and soil moisture dataset at 0.1° resolution from 1980 to near present. Sci Data 12. Doi: 10.1038/s41597-025-04610-y.
Miralles, D.G., Van Den Berg, M.J., Gash, J.H., Parinussa, R.M., De Jeu, R.A.M., Beck, H.E., Holmes, T.R.H., Jiménez, C., Verhoest, N.E.C., Dorigo, W.A., Teuling, A.J., Johannes Dolman, A., 2014. El Niño–La Niña cycle and recent trends in continental evaporation. Nat. Clim. Change 4, 122–126. https://doi.org/10.1038/nclimate2068.
Mondal, S., Mishra, A., 2024. Quantifying the precipitation, evapotranspiration, and soil moisture network's interaction over global land surface hydrological cycle. Water Resour. Res. 60. https://doi.org/10.1029/2023wr034861.
Muñoz-Sabater, J., Dutra, E., Agustí-Panareda, A., Albergel, C., Arduini, G., Balsamo, G., Boussetta, S., Choulga, M., Harrigan, S., Hersbach, H., Martens, B., Miralles, D.G., Piles, M., Rodríguez-Fernández, N.J., Zsoter, E., Buontempo, C., Thépaut, J.-N., 2021. ERA5-Land: a state-of-the-art global reanalysis dataset for land applications. Earth Syst. Sci. Data 13, 4349–4383. https://doi.org/10.5194/essd-13-4349-2021.
Oki, T., Kanae, S., 2006. Global hydrological cycles and world water resources. Science 313, 1068–1072. https://doi.org/10.1126/science.1128845.
Padrón, R.S., Gudmundsson, L., Decharme, B., Ducharne, A., Lawrence, D.M., Mao, J., Peano, D., Krinner, G., Kim, H., Seneviratne, S.I., 2020. Observed changes in dry-season water availability attributed to human-induced climate change. Nat. Geosci. 13, 477–481. https://doi.org/10.1038/s41561-020-0594-1.
Palácios, R., Castagna, D., Barbosa, L., Souza, A.P., Imbiriba, B., Zolin, C.A., Nassarden, D., Duarte, L., Morais, F.G., Franco, M.A., Cirino, G., Kuhn, P., Sodré, G., Curado, L., Basso, J., Roberto De Paulo, S., Rodrigues, T., 2024. ENSO effects on the relationship between aerosols and evapotranspiration in the south of the Amazon biome. Environ. Res. 250, 118516. https://doi.org/10.1016/j.envres.2024.118516.
Pan, S., Pan, N., Tian, H., Friedlingstein, P., Sitch, S., Shi, H., Arora, V.K., Haverd, V., Jain, A.K., Kato, E., Lienert, S., Lombardozzi, D., Nabel, J.E.M.S., Ottlé, C., Poulter, B., Zaehle, S., Running, S.W., 2020. Evaluation of global terrestrial evapotranspiration using state-of-the-art approaches in remote sensing, machine learning and land surface modeling. Hydrol. Earth Syst. Sci. 24, 1485–1509. https://doi.org/10.5194/hess-24-1485-2020.
Pan, S., Tian, H., Dangal, S.R.S., Yang, Q., Yang, J., Lu, C., Tao, B., Ren, W., Ouyang, Z., 2015. Responses of global terrestrial evapotranspiration to climate change and increasing atmospheric CO_2 in the 21st century. Earth's Future 3, 15–35. https://doi.org/10.1002/2014ef000263.
Papanatsiou, M., Petersen, J., Henderson, L., Wang, Y., Christie, J.M., Blatt, M.R., 2019. Optogenetic manipulation of stomatal kinetics improves carbon assimilation, water use, and growth. Science 363 (6434), 1456–1459. https://doi.org/10.1126/science.aaw0046.
Park, H., Jeong, S., Peñuelas, J., 2020. Accelerated rate of vegetation green-up related to warming at northern high latitudes. Glob. Chang. Biol. 26, 6190–6202. https://doi.org/10.1111/gcb.15322.
Pi, K., Bieroza, M., Brouchkov, A., Chen, W., Dufour, L.J.P., Gongalsky, K.B., Herrmann, A.M., Krab, E.J., Landesman, C., Laverman, A.M., Mazei, N., Mazei, Y., Öquist, M.G., Peichl, M., Pozdniakov, S., Rezanezhad, F., Roose-Amsaleg, C., Shatilovich, A., Shi, A., Smeaton, C.M., Tong, L., Tsyganov, A.N., Van Cappellen, P., 2021. The cold region critical zone in transition: responses to climate warming and land use change. Annu. Rev. Env. Resour. 46, 111–134. https://doi.org/10.1146/annurev-environ-012220-125703.
Piao, S., Nan, H., Huntingford, C., Ciais, P., Friedlingstein, P., Sitch, S., Peng, S., Ahlström, A., Canadell, J.G., Cong, N., Levis, S., Levy, P.E., Liu, L., Lomas, M.R., Mao, J., Myneni, R.B., Peylin, P., Poulter, B., Shi, X., Yin, G., Viovy, N., Wang, T., Wang, X., Zaehle, S., Zeng, N., Zeng, Z., Chen, A., 2014. Evidence for a weakening relationship between interannual temperature variability and northern vegetation activity. Nat. Commun. 5 (1). https://doi.org/10.1038/ncomms6018.
Piao, S., Wang, X., Park, T., Chen, C., Lian, X., He, Y., Bjerke, J.W., Chen, A., Ciais, P., Tømmervik, H., Nemani, R.R., Myneni, R.B., 2019. Characteristics, drivers and feedbacks of global greening. Nat. Rev. Earth Environ. 1, 14–27. https://doi.org/10.1038/s43017-019-0001-x.
Purdy, A.J., Fisher, J.B., Goulden, M.L., Colliander, A., Halverson, G., Tu, K., Famiglietti, J.S., 2018. SMAP soil moisture improves global evapotranspiration. Remote Sens. Environ. 219, 1–14. https://doi.org/10.1016/j.rse.2018.09.023.
Scanlon, B.R., Fakhreddine, S., Rateb, A., De Graaf, I., Famiglietti, J., Gleeson, T., Grafton, R.Q., Jobbagy, E., Kebede, S., Kolusu, S.R., Konikow, L.F., Long, D., Mekonnen, M., Schmied, H.M., Mukherjee, A., MacDonald, A., Reedy, R.C., Shamsudduha, M., Simmons, C.T., Sun, A., Taylor, R.G., Villholth, K.G., Vörösmarty, C.J., Zheng, C., 2023. Global water resources and the role of groundwater in a resilient water future. Nat. Rev. Earth Environ. 4, 87–101. https://doi.org/10.1038/s43017-022-00378-6.
Seneviratne, S.I., Corti, T., Davin, E.L., Hirschi, M., Jaeger, E.B., Lehner, I., Orlowsky, B., Teuling, A.J., 2010. Investigating soil moisture–climate interactions in a changing climate: a review. Earth Sci. Rev. 99, 125–161. https://doi.org/10.1016/j.earscirev.2010.02.004.
Shang, S., Zhu, G., Zhang, K., Chen, H., Wang, Y., Chen, Y., Zhang, Z., Ma, N., 2024. Spatial-temporal variations in evapotranspiration across the continental United States: an atmospheric water balance perspective. J. Hydrol. 640, 131699. https://doi.org/10.1016/j.jhydrol.2024.131699.
Swann, A.L., Fung, I.Y., Levis, S., Bonan, G.B., Doney, S.C., 2010. Changes in Arctic vegetation amplify high-latitude warming through the greenhouse effect. PNAS 107, 1295–1300. https://doi.org/10.1073/pnas.0913846107.
Tang, R., Peng, Z., Liu, M., Li, Z.-L., Jiang, Y., Hu, Y., Huang, L., Wang, Y., Wang, J., Jia, L., Zheng, C., Zhang, Y., Zhang, K., Yao, Y., Chen, X., Xiong, Y., Zeng, Z., Fisher, J.B., 2024. Spatial-temporal patterns of land surface evapotranspiration from global products. Remote Sens. Environ. 304, 114066. https://doi.org/10.1016/j.rse.2024.114066.
Tang, T., Ge, J., Shi, H., Wang, L., Cao, J.J., Lee, X.H., 2025. Drought frequency, intensity, and exposure have increased due to historical land use and land cover changes. Commun. Earth Environ. 6, 398. https://doi.org/10.1038/s43247-025-02392-0.
Teuling, A.J., Van Loon, A.F., Seneviratne, S.I., Lehner, I., Aubinet, M., Heinesch, B., Bernhofer, C., Grünwald, T., Prasse, H., Spank, U., 2013. Evapotranspiration amplifies European summer drought. Geophys. Res. Lett. 40, 071–2075. https://doi.org/10.1002/grl.50495.
Tito, T.M., Delgado, R.C., De Carvalho, D.C., Teodoro, P.E., De Almeida, C.T., Da Silva Junior, C.A., Dos Santos, E.B., Da Silva Júnior, L.A.S., 2020. Assessment of evapotranspiration estimates based on surface and satellite data and its relationship with El Niño–Southern Oscillation in the Rio de Janeiro State. Environ. Monit. Assess. 192. https://doi.org/10.1007/s10661-020-08421-z.
Vicente-Serrano, S.M., Domínguez-Castro, F., Beguería, S., El Kenawy, A., Gimeno-Sotelo, L., Franquesa, M., Azorin-Molina, C., Andres-Martin, M., Halifa-Marín, A., 2025. Atmospheric drought indices in future projections. Nat. Water 1–14. https://doi.org/10.1038/s44221-025-00416-9.
Vicente-Serrano, S.M., Miralles, D.G., McDowell, N., Brodribb, T., Domínguez-Castro, F., Leung, R., Koppa, A., 2022. The uncertain role of rising atmospheric CO2 on global plant transpiration. Earth Sci. Rev. 230, 104055. https://doi.org/10.1016/j.earscirev.2022.104055.
Volk, J.M., Huntington, J.L., Melton, F.S., Allen, R., Anderson, M., Fisher, J.B., Kilic, A., Ruhoff, A., Senay, G.B., Minor, B., Morton, C., Ott, T., Johnson, L., Comini De Andrade, B., Carrara, W., Doherty, C.T., Dunkerly, C., Friedrichs, M., Guzman, A., Hain, C., Halverson, G., Kang, Y., Knipper, K., Laipelt, L., Ortega-Salazar, S., Pearson, C., Parrish, G.E.L., Purdy, A., ReVelle, P., Wang, T., Yang, Y., 2024. Assessing the accuracy of OpenET satellite-based evapotranspiration data to support water resource and land management applications. Nat. Water 2, 193–205. https://doi.org/10.1038/s44221-023-00181-7.
Wang, R., Li, L., Gentine, P., Zhang, Y., Chen, J., Chen, X., Chen, L., Ning, L., Yuan, L., Lü, G., 2022. Recent increase in the observation-derived land evapotranspiration due

to global warming. Environ. Res. Lett. 17, 024020. https://doi.org/10.1088/1748-9326/ac4291.
Wang, Y., Cao, G., Wang, Y., Webb, A.A., Yu, P., Wang, X., 2019. Response of the daily transpiration of a larch plantation to variation in potential evaporation, leaf area index and soil moisture. Sci. Rep. 9. https://doi.org/10.1038/s41598-019-41186-1.
Wang, Y.X., Peng, L., Y, Y.M., Chen, T.T., 2024. Global vegetation-temperature sensitivity and its driving forces in the 21st century. Earth's Future 12, e2022EF003395. https://doi.org/10.1029/2022EF003395.
Winkler, K., Fuchs, R., Rounsevell, M., Herold, M., 2021. Global land use changes are four times greater than previously estimated. Nat. Commun. 12. https://doi.org/10.1038/s41467-021-22702-2.
Xue, Y., Zhang, Z., Li, X., Liang, H., Yin, L., 2025. A review of evapotranspiration estimation models: advances and future development. Water Resour. Manag. 39, 3641–3657. https://doi.org/10.1007/s11269-025-04191-w.
Yan, H., Yu, Q., Zhu, Z., Myneni, R.B., Yan, H.-M., Wang, S., Shugart, H.H., 2013. Diagnostic analysis of interannual variation of global land evapotranspiration over 1982–2011: assessing the impact of ENSO. JGR Atmospheres 118, 8969–8983. https://doi.org/10.1002/jgrd.50693.
Yang, Y., Roderick, M.L., Guo, H., Miralles, D.G., Zhang, L., Fatichi, S., Luo, X., Zhang, Y., McVicar, T.R., Tu, Z., Keenan, T.F., Fisher, J.B., Gan, R., Zhang, X., Piao, S., Zhang, B., Yang, D., 2023. Evapotranspiration on a greening Earth. Nat. Rev. Earth Environ. 4, 626–641. https://doi.org/10.1038/s43017-023-00464-3.
Yang, Z., Zhang, Q., Hao, X., Yue, P., 2019. Changes in evapotranspiration over global semiarid regions 1984–2013. J. Geophys. Res. Atmos. 124, 2946–2963. https://doi.org/10.1029/2018JD029533.
Yao, J., Liu, H., Huang, J., Gao, Z., Wang, G., Li, D., Yu, H., Chen, X., 2020. Accelerated dryland expansion regulates future variability in dryland gross primary production. Nat. Commun. 11 (1), 1665. https://doi.org/10.1038/s41467-020-15515-2.
Zeng, Z., Peng, L., Piao, S., 2018. Response of terrestrial evapotranspiration to Earth's greening. Curr. Opin. Environ. Sustain. 33, 9–25. https://doi.org/10.1016/j.cosust.2018.03.001.
Zhang, A., Jia, G., 2020. ENSO-driven reverse coupling in interannual variability of pantropical water availability and global atmospheric CO_2 growth rate. Environ. Res. Lett. 15, 034006. https://doi.org/10.1088/1748-9326/ab66cc.
Zhang, K., Chen, H., Ma, N., Shang, S., Wang, Y., Xu, Q., Zhu, G., 2024. A global dataset of terrestrial evapotranspiration and soil moisture dynamics from 1982 to 2020. Sci. Data 11. https://doi.org/10.1038/s41597-024-03271-7.
Zhang, K., Kimball, J.S., Kim, Y., McDonald, K.C., 2011. Changing freeze-thaw seasons in northern high latitudes and associated influences on evapotranspiration. Hydrol. Process. 25, 4142–4151. https://doi.org/10.1002/hyp.8350.
Zhang, K., Kimball, J.S., Nemani, R.R., Running, S.W., Hong, Y., Gourley, J.J., Yu, Z., 2015. Vegetation greening and climate change promote multidecadal rises of global land evapotranspiration. Sci. Rep. 5. https://doi.org/10.1038/srep15956.
Zhang, K., Kimball, J.S., Running, S.W., 2016. A review of remote sensing based actual evapotranspiration estimation. WIREs Water 3, 834–853. https://doi.org/10.1002/wat2.1168.
Zhang, X., Zhang, Y., Ma, N., Kong, D., Tian, J., Shao, X., Tang, Q., 2021. Greening-induced increase in evapotranspiration over Eurasia offset by CO_2-induced vegetational stomatal closure. Environ. Res. Lett. 16, 124008. https://doi.org/10.1088/1748-9326/ac3532.
Zhang, Y., Li, C., Chiew, F.H.S., Post, D.A., Zhang, X., Ma, N., Tian, J., Kong, D., Leung, L. R., Yu, Q., Shi, J., Liu, C., 2023. Southern Hemisphere dominates recent decline in global water availability. Science 382, 579–584. https://doi.org/10.1126/science.adh0716.
Zhang, Y., Ma, N., Park, H., Walsh, J.E., Zhang, K., 2020. Evaporation processes and changes over the northern regions. In: Arctic Hydrology, Permafrost and Ecosystems. Springer International Publishing, Cham, pp. 101–131.
Zhao, M., A, G., Liu, Y., Konings, A.G., 2022. Evapotranspiration frequently increases during droughts. Nat. Clim. Chang. 12, 1024–1030. https://doi.org/10.1038/s41558-022-01505-3.
Zhou, S., Williams, A.P., Lintner, B.R., Berg, A.M., Zhang, Y., Keenan, T.F., Cook, B.I., Hagemann, I., Seneviratne, S.I., Gentine, P., 2021. Soil moisture–atmosphere feedbacks mitigate declining water availability in drylands. Nat. Clim. Chang. 11, 38–44. https://doi.org/10.1038/s41558-020-00945-z.
Zhu, G., Zhang, K., Chen, H., Wang, Y., Su, Y., Zhang, Y., Ma, J., 2019. Development and evaluation of a simple hydrologically based model for terrestrial evapotranspiration simulations. J. Hydrol. 577, 123928. https://doi.org/10.1016/j.jhydrol.2019.123928.
Zhu, W., Zhao, D., Di, N., Li, D., Zhou, O., Sun, Y., Jia, L., Ding, C., Xi, B., 2023. Matching root water uptake patterns to fine root and soil water distributions. Plant and Soil 495, 499–516. https://doi.org/10.1007/s11104-023-06349-0.
Zhu, Y., Zheng, Z., Zhao, G., Zhu, J., Zhao, B., Sun, Y., Gao, J., Zhang, Y., 2025. Evapotranspiration increase is more sensitive to vegetation greening than to vegetation type conversion in arid and semi-arid regions of China. Global Planet. Change 244, 104634. https://doi.org/10.1016/j.gloplacha.2024.104634.
Zou, M., Yang, K., Lu, H., Ren, Y., Sun, J., Wang, H., Tan, S., Zhao, L., 2023. Integrating eco-evolutionary optimality principle and land processes for evapotranspiration estimation. J. Hydrol. 616, 128855. https://doi.org/10.1016/j.jhydrol.2022.128855.